geosciences

MDPI

Article

Superposed Sedimentary and Tectonic Block-In-Matrix Fabrics in a Subducted Serpentinite Mélange (High-Pressure Zermatt Saas Ophiolite, Western Alps)

Paola Tartarotti [1,*], Sara Guerini [1], Francesca Rotondo [1], Andrea Festa [2], Gianni Balestro [2], Gray E. Bebout [3], Enrico Cannaò [1,4], Gabe S. Epstein [3] and Marco Scambelluri [5]

1 Dipartimento di Scienze della Terra, Università degli Studi di Milano, via Mangiagalli 34, 20133 Milano, Italy
2 Dipartimento di Scienze della Terra, Università di Torino, Via Valperga Caluso 35, 10125 Torino, Italy
3 Department of Earth and Environmental Sciences, Lehigh University, Bethlehem, PA 18015, USA
4 Istituto di Geoscienze e Georisorse, CNR, Via Moruzzi 1, 56124 Pisa, Italy
5 Dipartimento di Scienze della Terra Ambiente e Vita, Università di Genova, Corso Europa, 26, 16132 Genova, Italy
* Correspondence: paola.tartarotti@unimi.it

Received: 6 July 2019; Accepted: 13 August 2019; Published: 16 August 2019

Abstract: The primary stratigraphic fabric of a chaotic rock unit in the Zermatt Saas ophiolite of the Western Alps was reworked by a polyphase Alpine tectonic deformation. Multiscalar structural criteria demonstrate that this unit was deformed by two ductile subduction-related phases followed by brittle-ductile then brittle deformation. Deformation partitioning operated at various scales, leaving relatively unstrained rock domains preserving internal texture, organization, and composition. During subduction, ductile deformation involved stretching, boudinage, and simultaneous folding of the primary stratigraphic succession. This deformation is particularly well-documented in alternating layers showing contrasting deformation style, such as carbonate-rich rocks and turbiditic serpentinite metasandstones. During collision and exhumation, deformation enhanced the boudinaged horizons and blocks, giving rise to spherical to lozenge-shaped blocks embedded in a carbonate-rich matrix. Structural criteria allow the recognition of two main domains within the chaotic rock unit, one attributable to original broken formations reflecting turbiditic sedimentation, the other ascribable to an original sedimentary mélange. The envisaged geodynamic setting for the formation of the protoliths is the Jurassic Ligurian-Piedmont ocean basin floored by mostly serpentinized peridotites, intensely tectonized by extensional faults that triggered mass transport processes and turbiditic sedimentation.

Keywords: sedimentary mélange; broken formation; ophiolite; Zermatt Saas; turbidite

1. Introduction

In most orogenic belts and exhumed subduction-accretion complexes around the world, a strong morphological convergence of meso- to map-scale fabrics exists in the block-in-matrix fabric of different types of mélange (i.e., sedimentary, diapiric, tectonic, and polygenetic mélanges) [1–3]. This close resemblance has led to a long-standing debate on the nature and mode of geological processes (i.e., gravitational vs. tectonics), that lead to the formation of chaotic rock assemblages, particularly in areas of well-preserved, exhumed subduction-accretion complexes such as in the Western US Cordillera, the Circum-Pacific Region, and Circum-Mediterranean Region [1–20]. In fact, the mechanisms responsible for the formation of mélanges may occur in a wide range of geological settings, ranging from relatively shallow to deep crustal levels [7,21]. Thus, the ongoing debate revolves

around whether the "chaotic disruption and mixing" of rock assemblages, observed in exhumed orogenic belts and subduction-accretion complexes, is a result of tectonic shearing alone, achieved at different depths, or a product of tectonic reworking and "recycling" of mass transport deposits (MTDs) during the overall geodynamic evolution [7,15,22]. Further complications arise from the degree of heterogeneity of the primary lithostratigraphic units involved in the tectonic processes (i.e., subduction and/or orogenetic processes) forming chaotic rock units. Among others, a notable example is the Ocean Plate Stratigraphy (OPS) mélange resulting from the fragmentation, disruption and/or mixing of different types of widely varying lithologies deposited in oceanic settings [7,22–27].

In the Western Alps, chaotic rock units and mélanges including metaophiolitic and/or continental basement and mantle blocks or slivers have been differently interpreted as remnants of an exhumed "subduction channel" (as defined by reference [28]) or subduction-related mélange [29–31], or alternatively, as the product of inherited intraoceanic (i.e., pre-Alpine) deformation [17,19,32]. This range of interpretations, likely reflecting the exposure of chaotic units in various stages of evolution (from the pre-orogenic stage to subduction and subsequent collision) may not be contradictory, particularly for serpentinite-matrix mélanges derived by the dismemberment of metaophiolitic sequences. The latter derive from the closure of the Jurassic Tethyan ocean beginning in the Late Cretaceous ([33–37] and references therein). These metaophiolites show various rock assemblages and metamorphic imprints related to the Alpine orogenic cycle (subduction followed by collision-related exhumation). Records of the oceanic evolution are still locally preserved, in the form of relict structural and mineralogical features ([38–41] and references therein). The well-known metaophiolites of the NW Alps include the Zermatt Saas and the Combin Zones [42,43]. The Zermatt-Saas Zone comprises dominant serpentinized peridotites with metagabbros and rodingitic dikes, metabasalts, associated with a metasedimentary cover consisting of metaquartzites, marble, and calcschists, all showing effects of high pressure (HP) to ultra high pressure (UHP) subduction-related Alpine metamorphism [44–54]. The Combin Zone consists of carbonate and terrigeneous flysch-type calcschists hosting tectonic sheets of metamafic and ultramafic rocks. The dominant Alpine metamorphic mineral assemblages developed under greenschists facies, during exhumation, although a few blueschists-facies relics are also preserved [44,55–58].

In this paper, we focus on the description of a serpentinite chaotic rock unit (the "Composite Chaotic Unit" of [19]) exposed in the high Champorcher valley (Aosta Valley region; Figure 1), occurring between a serpentinite and metaophicarbonate basement and a metasedimentary cover succession composed of post-rift calcschists. The "Composite Chaotic Unit" (CCU hereafter) consists of differing superimposed primary sedimentary mélanges and broken formations formed by the interplay of polyphasic tectonics and sedimentary processes. Sedimentary processes were triggered by active intra-oceanic (i.e., syn-rift) extensional faulting exposing mantle rocks on the seafloor of the Jurassic Tethyan ocean, producing mass-transport and resulting turbiditic sedimentation [19].

Beginning with the reconstruction of [19], which documented the gravitational sedimentation of parts of the CCU, we focus on the roles played by the Alpine subduction and collisional tectonics recorded by map- to micro-scale structures. We evaluate the impact of polyphasic Alpine tectonic deformation (subduction followed by collision-related exhumation) in reworking and reorganizing the primary fabric of Jurassic mass-transport and turbidite deposition, and resulting in the chaotic rock assemblage presently exposed in the CCU. This investigation of the Champorcher valley metaophiolite and the CCU sheds light on the origin of similar peculiar chaotic rock assemblages in the NW Alps metaophiolites and ophiolitic belts. The concurrent presence of serpentinites, chaotic rock units, and carbonate-rich rocks represents a key manifestation on the geodynamics of ophiolites involved in subduction, and can yield insight into mélange formation and the roles of fluids in such settings.

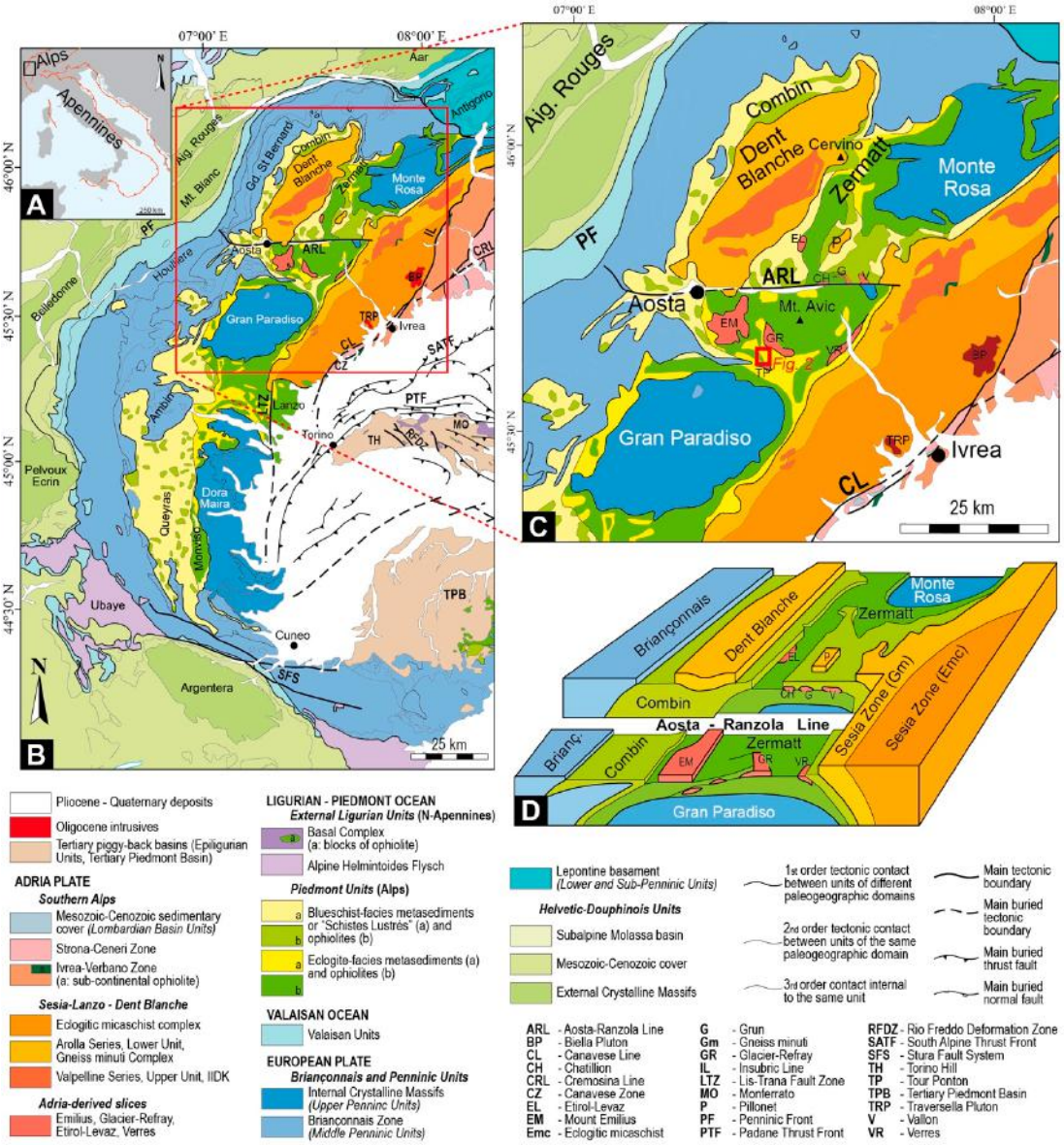

Figure 1. Geographic and geological location of the study area. (**A**) Location of the W Alps and the study area (square) in the Italian peninsula. (**B**) Tectonic map of the W Alpine belt illustrating the distribution of the tectonic domains involved in the Alpine orogeny (see text). Red square outlines the area zoomed in Figure 1C. (**C**) Tectonic map of the Aosta valley and surrounding areas, with location of the study area (mapped in Figure 2) and of the Mount Avic serpentinite massif (M. Avic). (**D**) 3D-block diagram across the Aosta-Ranzola fault system (Aosta-Ranzola Line) trending parallel to the central Aosta valley. Figure 1A–C: modified after [59]. Figure 1D: redrawn after [33].

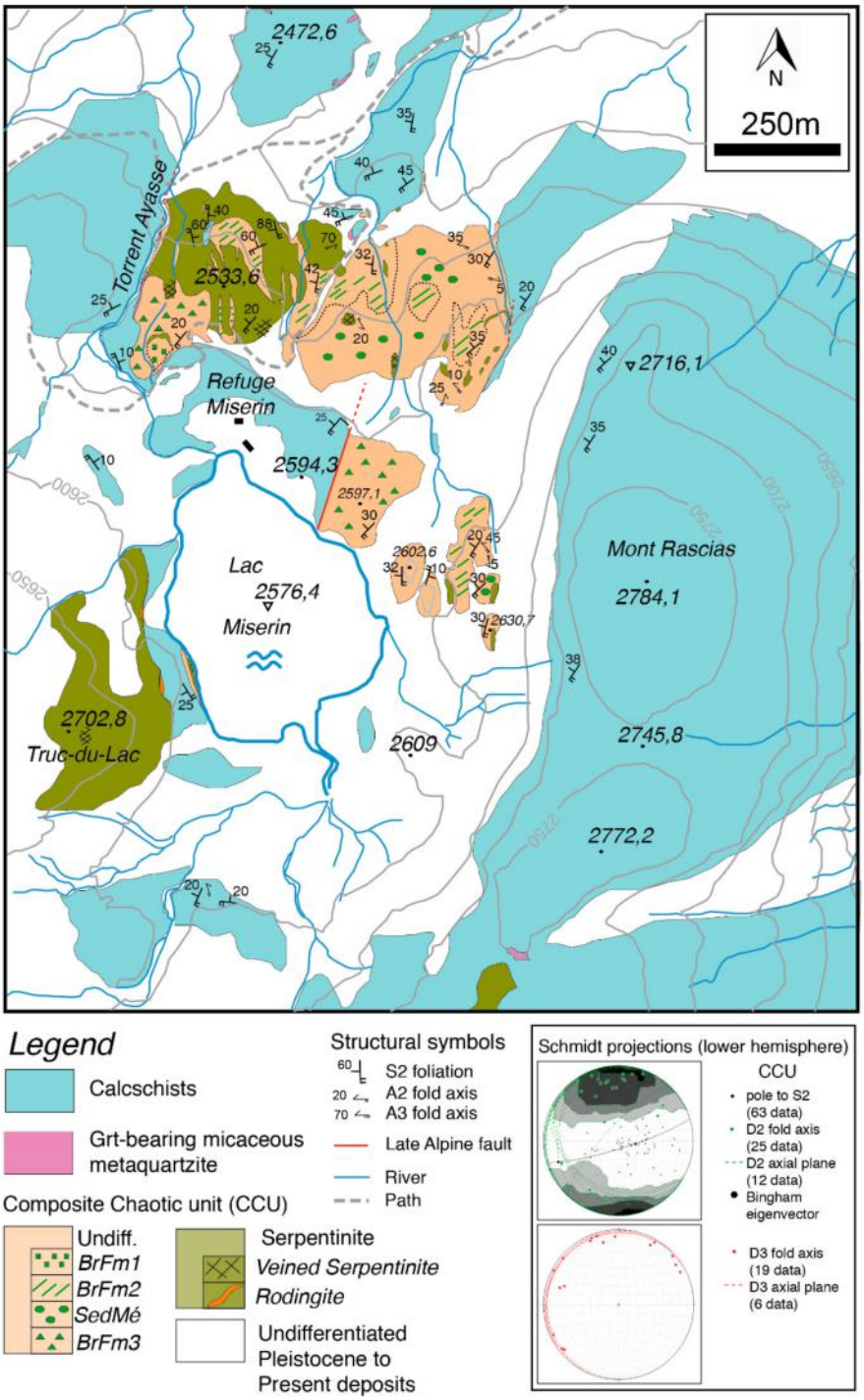

Figure 2. Geological map of the study area (from original field mapping at 1:5000 scale) and lower hemisphere projections of the main structural fabrics.

2. Regional Geological Background

The Alps are the aggregate result of convergent-margin processes beginning in the Late Cretaceous and affecting the palaeo-European and Adriatic plates. The convergence led to the subduction of part of the continental passive margin, the progressive closure of an ocean basin (i.e., the Jurassic Tethyan ocean), and, ultimately, continental collision in the Cenozoic [33,36,60–66]. The subduction process, best represented in the W Alps in occurrences of blueschist- and eclogite-facies rocks, affected the innermost units derived from the Adria domain, then progressively the more external units

derived from the oceanic domain and from the European passive margin. Radiometric ages for peak-pressure metamorphism during the subduction show a wide time span ranging between ca. 80 and 42 Ma [33,34,67–70] in both the continental and ophiolitic units, suggesting that the subducted tectonic units in the W Alps attained their maximum P–T imprint diachronously. This interpretation is supported by simulations of the ocean-continent dynamics performed by numerical modeling [71,72].

In the W Alps, metaophiolites occur in several tectonic units, including the eclogite-facies Zermatt-Saas Zone [42,43,73], the Grivola-Urtier unit [74] (see e.g., reference [75] and references therein), the Monviso ophiolite complex [32,76,77], and the blueschist/greenschist-facies Combin Zone, Queyras, and Corsica ophiolite units [78–80]. These units are distinct for their Alpine metamorphic evolution and for their internal structure and rock assemblage and they represent the fossil oceanic lithosphere of the Jurassic Tethyan ocean [43,44]. This ocean basin, separating the continental Adriatic/African and European plates, consisted of a main branch known as the Piemonte-Ligurian (or South Penninic) basin, and minor northern branches including the Valaisan (or North Penninic; e.g., see [81–84]), and the Antrona basins [85–87]. These latter two sub-basins were separated by the Briançonnais peninsula preserved in the W Alps [84,88,89] but thinned to the east, so that only one Penninic ocean basin gave rise rise to the ophiolites exposed in the E Alps at/near the Tauern tectonic window [90] (see also the review in [91]). This setting is thought to have resulted from an intense fragmentation of the oceanic spreading ridge promoted by regional-scale transform faults, as envisaged in several paleogeographic reconstructions [83,89,92]. The Zermatt-Saas Zone, which can be correlated with the metaophiolites in our study area, consists of typical units of Atlantic-type (slow-spreading) oceanic crust, including ultramafic rocks, metagabbros, and metabasalts with locally preserved sedimentary cover sequences [43,93]. Most lithologies of the Zermatt-Saas Zone display high-pressure (HP) to ultra-high (UHP) mineral assemblages [44–46,48,52,94].

The High Champorcher Valley Ophiolite

The study area is located in the high Champorcher Valley (NW Alps), in the Italian side of the Graian Alps, to the south of the Aosta-Ranzola fault system (Figure 1). In this area, several units of both continental and oceanic origin are tectonically juxtaposed [95–99]. Metaophiolites mainly consist of serpentinites with metarodingitic dykes, metamafic rocks (mostly metagabbros), mafic and metaophicarbonate breccias, and a metasedimentary cover dominated by flysch-type calcschists [40,41,74,100]. Serpentinites are widely exposed in the north of the Champorcher valley, in the Mount Avic area where they constitute a huge massif of ca. 180 km^2 [74,100] (Figure 1C). These rocks derive from a mantle peridotite protolith and are characterized by Alpine HP mineral parageneses including olivine, Ti-clinohumite, serpentine group minerals, magnetite, and by rare pre-Alpine (oceanic) mineral relics [40,41,100]. Serpentinites are often associated with metaophicarbonate breccias demonstrating seafloor exposure of mantle rocks during the Jurassic ocean spreading [19,101,102]. Metaophiolite units are in tectonic contact with the eclogitic Lower Austroalpine "outliers" of the Tour Ponton, Glacier-Refray, and other minor slivers [74,103]; the European-related continental domain is here represented by the northern sector of the Gran Paradiso massif exposed to the south of the Champorcher valley (Figure 1C).

3. Methods

Common techniques of field mapping were utilized for this study and supported by structural analyses at the outcrop and micro-scale. Criteria for identifying structural overprinting were adopted on the basis of common deformation patterns and/or similar mineral paragenesis (further constrained petrographically). Numbering of deformation phases (e.g., D_1–D_3) and related structures (e.g., S_1–S_3, etc.), was employed to distinguish the local chronology of the structures.

Our microstructural analysis was aimed at defining the relationships between deformation and metamorphism. Towards this goal, the sampling strategy was arranged so that, for each lithotype, a representative sample was analyzed to cover the full range of lithological variability from each

unit (clasts, matrices, clast/matrix contacts, veins, and vein infill inside boudin necks). Schematic relationships between deformation and mineral crystallization in the metaophiolite sequence are reported in Table S1. Mineral abbreviations adopted throughout the text are taken from [104] except for white mica (Wm). Additional details on the methodologies and criteria adopted in this study can be found in the Text S1. In the following, we refer to Festa et al. (2019a; see [4]) for the used mélange terminology.

4. The Composite Chaotic Unit (CCU)

In the high Champorcher valley, a peculiar metaophiolite sequence is exposed near Lake Miserin (i.e., the "Lake Miserin Ophiolite" or "LMO" of [19]). This sequence is characterized by the occurrence of the CCU, a polygenetic serpentinite chaotic rock unit, which is directly interposed between a variably foliated serpentinite basement units and a metasedimentary cover unit (Figures 2 and 3).

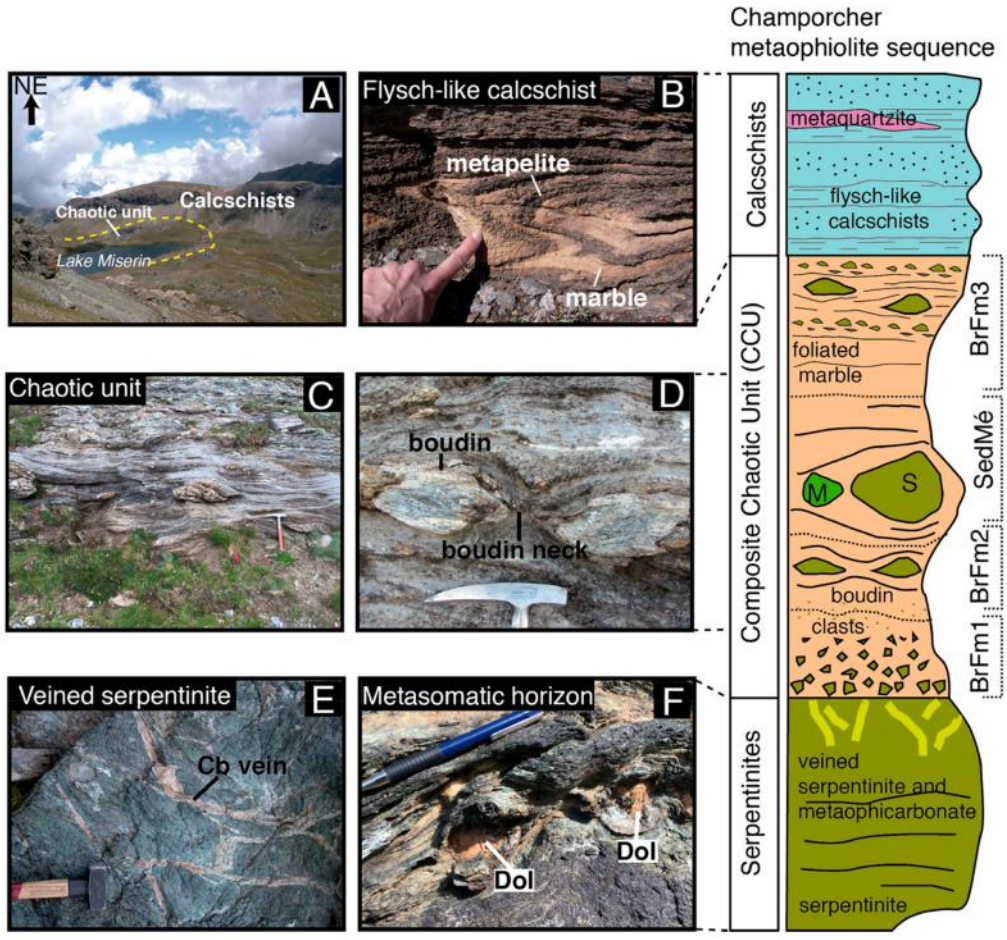

Figure 3. Panoramic and outcrop views of the Champorcher valley metaophiolite sequence near Lake Miserin. The main reconstructed stratigraphy of the Composite Chaotic Unit (CCU) is synthetized in the stratigraphic section (to the right). (**A**) Panoramic view of the CCU and overlying calcschists near Lake Miserin (high Champorcher valley). (**B**) Outcrop view of the calschist unit characterized by compositional layering defined by alternating metapelite and marble (interpreted to derive from an original bedding S0 of a flyschoid sequence; see text). (**C**) Block-in-matrix fabric of the CCU consisting of ultramafic blocks and clasts embedded in Cb-rich or calcschist foliated matrix. (**D**) Close-up of boudinaged ultramafic clasts in the CCU. (**E**) Top part of the serpentinite basement cut by Cb-rich veins ("veined serpentinites"). (**F**) Outcrop view of the metasomatic horizon at the contact between the CCU and underlying serpentinite.

Serpentinites are composed of Srp, Mag, ± Di ± Am (Tr) ± Chl ± Ep. Rodingite rims are locally developed along the contact between serpentinites and calcschists (see Figure 2). Serpentinites have been carbonated to various extents, mostly by development of Cb-rich vein networks. Foliated serpentinites show thin intrafolial Cb-rich layers, whereas in the massive type, Srp is associated with patchy Cb. A transition exists between pure serpentinites and "veined" serpentinites, marked by a gradual increase in the number of veins, filled with fibrous Srp or Cb (Figure 3E). The Cb-rich serpentinites are defined as ophicarbonate [105], that in the study area are made of serpentinites or metasomatized serpentinites, composed of Chl + Am ± Ep ± Mag ± Tlc. They have developed a diffused network of millimeter to centimeter-thick veins, filled with Cal, Dol, and minor Mgs. Cb-bearing veins occur both sub-parallel and at high-angles to the main foliation, giving rise to rhombohedral portions or irregular blocks of serpentinite.

The veined serpentinites and ophicarbonates are usually adjacent to a metasomatic horizon with a gradual and irregular contact. Rocks within this horizon typically show millimeter-thick layers of Amp (Act-Tr) ± Chl alternating with layers of carbonate minerals. These green- and orange-colored layers define a foliation that broadly characterizes the metasomatic horizon (Figure 3F). In less deformed portions of the CCU, the metasomatic horizon consists of boudins of serpentinite, Chl-rich schists, and boudins of Cb, variably associated with Di fibers. Where present, the Di fibers extend parallel to the main foliation. Consequently, the foliation visible at the outcrop scale in the metasomatic horizon is either irregular or parallel and concordant to the contacts with the overlying and underlying lithologies.

The CCU shows a block-in-matrix fabric, and has a thickness of ca. 40 m although it tapers out from east to west [19] showing a wedge-shaped architecture. It consists of four main types of chaotic rock-units with different block-in-matrix fabric. Individual units are distinguished on the basis of composition, proportion of clasts to matrix material, and shape of clasts/blocks. With reference to a reconstructed stratigraphy [19] we encountered from bottom to top the following rock-units (Figures 4 and 5):

- Broken formation 1 (BrFm1), consisting of clast-supported ultramafic metabreccia;
- Broken formation 2 (BrFm2), made of decimeter-thick horizons of ultramafic metabreccia and metasandstone embedded in a carbonate-rich matrix;
- Sedimentary mélange (SedMé), consisting of rounded to irregular exotic mafic and ultramafic blocks embedded within a marble matrix;
- Broken formation 3 (BrFm3), consisting of decimeters-thick horizons of ultramafic metabreccia and metasandstone embedded in a calcschist and marble matrix.

4.1. BrFm1

The BrFm1 is exposed in the western sector of the map area (see Figure 2) and has a thickness of 2–3 m. It directly overlies serpentinite and is in sharp contact with overlying BrFm3 or calcschists (see also [19]). The BrFm1 consists of a clast- to matrix-supported ultramafic metabreccia, with irregular to subrounded clasts ranging in size from decimeters to centimeters (Figure 4A). Rare elongated or lense-shaped blocks up to 50 cm long may occur within the metabreccia. At the outcrop scale, this unit is characterized by both normal and reverse internal grading, probably resulting from tectonic repetition. At the microscale (see below), the brecciated texture is not always clearly recognizable, either due to replacement of the serpentinite component during carbonation, or where Alpine deformation has produced a compositional layering defined by Srp and Cb.

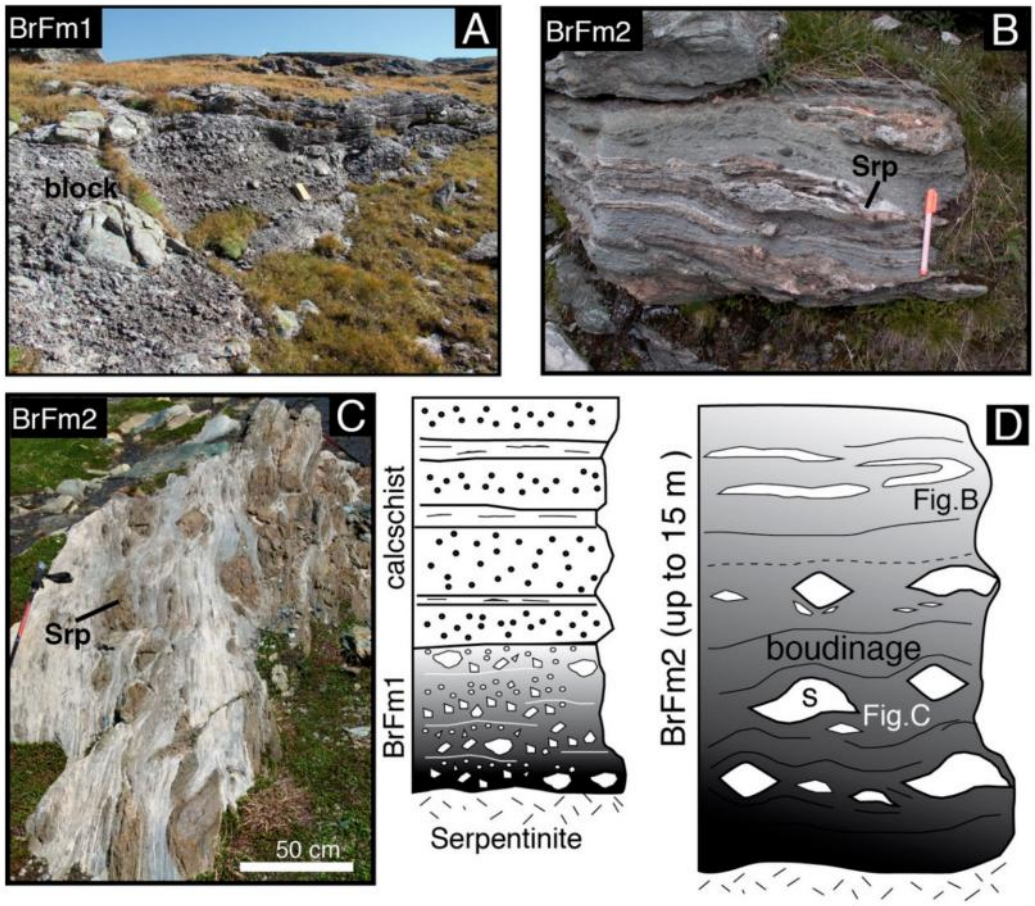

Figure 4. Outcrop views of Broken formation 1 (BrFm1) and Broken formation 2 (BrFm2) in the CCU of the high Champorcher valley. (**A**) BrFm1 outcrop exposed in the northwestern study area. It consists of clast- to matrix-supported ultramafic metabreccia with decimeter- to centimeter-sized clasts. Rare elongated or lense-shaped blocks up to 50 cm long (left side) may occur. At the outcrop scale, this unit is characterized by both normal and reverse internal grading. Notebook for scale. (**B**) BrFm2 outcrop showing disrupted horizons and clasts with ultramafic composition (covered by orange colored coating; Srp) embedded within a Cb-rich matrix. (**C**) View of the most common occurrence of BrFm2 characterized by a block-in-matrix fabric with boudinaged horizons, centimeter to decimeter thick, composed of ultramafic metasandstone (Srp), enveloped in an impure, white, or grey-colored matrix. Stick for scale. (**D**) Conceptual cartoon illustrating the internal fabric of the BrFm1 and BrFm2 units in relation with the surrounding rocks.

4.2. BrFm2

The BrFm2 is exposed in the northeastern sector of the study area (see Figure 2) and has a thickness of up to 15 m. It directly overlies the metaophicalcite and serpentinite with an intervening metasomatic horizon (Figure 4; see also Figure 3F), whereas the BrFm1 has never been observed at the base of BrFm2. The BrFm2 is characterized by a block-in-matrix fabric with boudinaged horizons (centimeter to decimeter thick), composed of medium- to coarse-grained ultramafic metasandstone, enveloped in an impure, white or grey-colored matrix (Figure 4B,C). Ultramafic micro-clasts and clasts, millimeter to centimeter wide, are locally distributed along thin horizons, which are aligned to boudinaged horizons. Both matrix and boudins are foliated, with the long axis of boudins being parallel or sub-parallel to the regional scale foliation (see the next section). The boudin internal foliation of most boudins is parallel to the matrix foliation, but sometimes it is developed at 30°–40° with respect to the boudin boundary, where it is dragged and becomes sub-parallel to the matrix foliation. Boudins within BrFm2 can be either symmetric or asymmetric. The neck zone connecting boudins is filled with fibrous or elongate

minerals such as Cpx or Cb. The ultramafic horizons are characterized by a regular and planar shape, but in most cases they derived from isoclinal folding parallel to the main foliation (see Figure 4B). The matrix of BrFm2 is an impure fine-grained marble characterized by alternating white cm-thick layers with a granoblastic texture, that encloses levels of grey marble and of fine-grained ultramafic breccia. Furthermore, the matrix may include centimeter-thick horizons of SedMé, suggesting that the two types show a transitional and/or gradational contact.

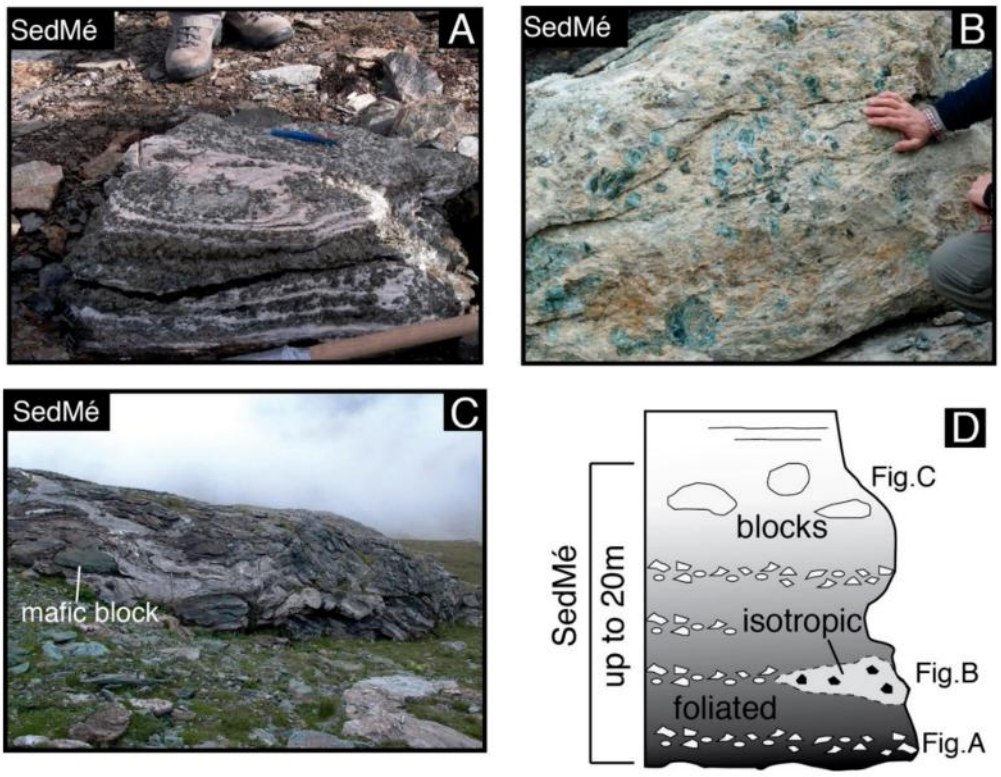

Figure 5. Outcrop views of the sedimentary mélange (SedMé) unit. (**A**) Clast-supported type showing a foliated texture defined by centimeter- to decimeter-thick horizons of metabreccia consisting of angular, subangular, or elongated clasts of serpentinite, embedded within a whitish Cb-rich matrix. Pen for scale. (**B**) Matrix-supported type characterized by an isotropic texture defined by a whitish-greenish matrix with disseminated ultramafic clasts composed of fibers of Srp growing radially from the centre of the clast. (**C**) Matrix-supported type including blocks of serpentinite, veined serpentinite or ophicarbonate, and mafic rocks. The mafic block is ca. 50 cm sized. (**D**) Conceptual cartoon illustrating the internal fabric of the SedMé unit.

4.3. SedMé

The SedMé is characterized by a block-in-matrix fabric, with irregular to subrounded clasts and exotic blocks with mafic and ultramafic composition, embedded in a whitish or grey Cb-rich matrix. It includes various types characterized by different clast-to-matrix ratio and different size of clasts. Clast-supported types commonly have a foliated texture (Figure 5A), the foliation being defined by centimeter- to decimeter-thick horizons of metabreccia consisting of angular, subangular, or elongated clasts of Srp. These horizons are embedded within a whitish Cb-rich matrix. Matrix-supported types are characterized by an isotropic texture defined by a whitish-greenish matrix with disseminated ultramafic clasts, devoid of any internal organization (Figure 5B). Single clasts are often composed of fibers of Srp growing radially from the center of the clast. The fibrous clasts show irregular shapes and have dimensions ranging from a few millimeters up to a few centimeters. Matrix-supported SedMé may also include blocks of serpentinite, veined serpentinite or ophicarbonate, and mafic rocks; these blocks are decimeters to 1 m in size and show a low aspect ratio (Figure 5C). The SedMé has

a wedge-like shaped geometry, ranging in thickness from few meters (to SW) up to 20 m (to NE). It grades to the upper BrFm3 by increasing the calcschist component of the matrix.

4.4. BrFm3

The BrFm3 represents the uppermost part of the CCU, it has an average thickness of ca. 10 m and is directly overlain by calcschists. This unit is exposed to the N and NE of Lake Miserin (see Figure 2) and, due to the general wedge-shaped geometry of the underlying units, it may be directly in contact with the metasomatic rocks near the serpentinite basement (Figure 6). The BrFm3 is comparable in composition to the BrFm2 described above, but it differs in the relatively higher amount of calcschist component in the matrix, consisting of an impure light-grey marble and calcschist, with diffuse, equal grain size, sub-centimeter ultramafic clasts (Figure 6B). Within the matrix, the foliation is marked by thin layers of relatively pure marble, alternating with thicker and more abundant layers rich in ultramafic metasandstone and rare clasts. Metasandstone layers show tabular and elongated shapes, very often boudinaged (Figure 6C,D) and consist of medium- to fine-grained ultramafic metasandstone (Srp ± Amp ± Chl ± Ep). Their internal foliation corresponds to a compositional layering marked by the juxtaposition of ultramafic dark green layers and whitish Chl ± Amp ± Cb layers. The internal foliation of blocks and boudins within the BrFm3 is parallel to and continuous with the matrix foliation.

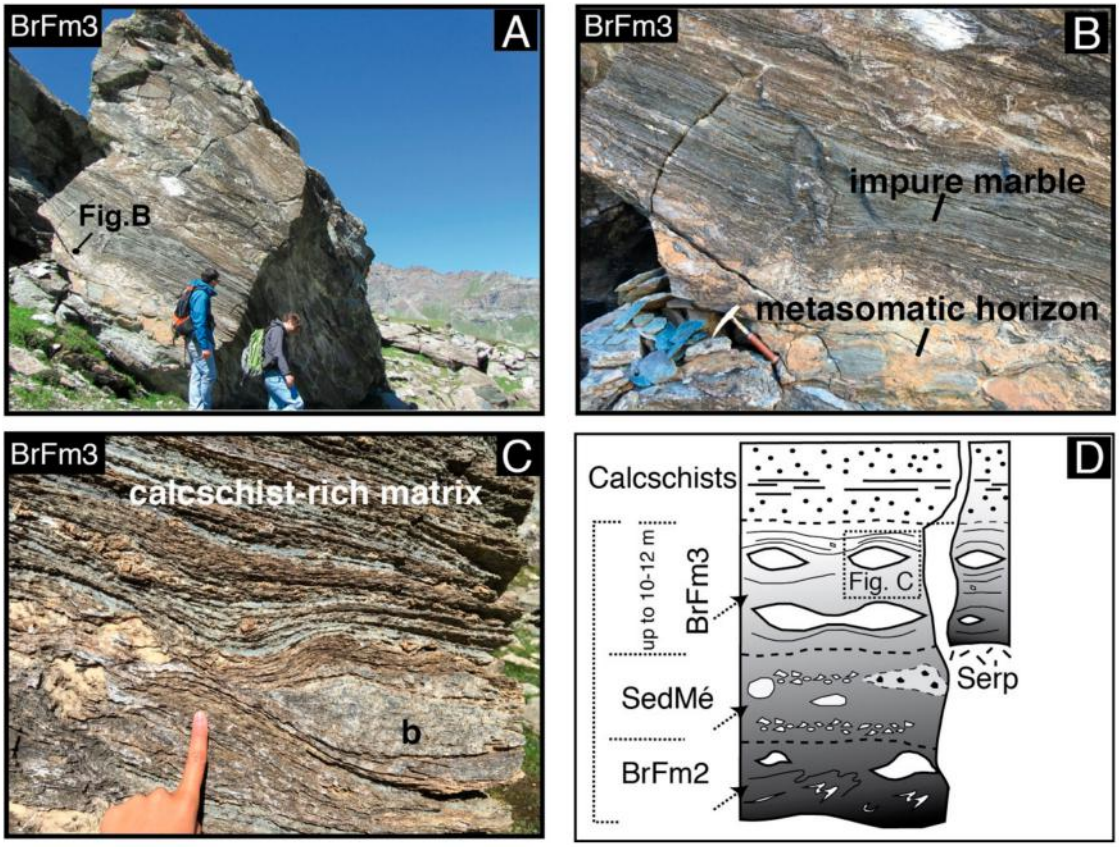

Figure 6. Outcrop views of Broken formation 3 (BrFm3) in the CCU. (**A**) General outcrop view of the BrFm3 exposed to the N and NE of Lake Miserin. (**B**) Contact between the impure marble and calcschist-rich matrix of the BrFm3 and the underlying metasomatic horizon. (**C**) Close-up of the boudinaged ultramafic metasandstone horizons (b) consisting of medium- to fine-grained ultramafic metasandstone (Srp ± Amp ± Chl ± Ep). (**D**) Conceptual cartoon illustrating the internal fabric of the BrFm3 unit in relation to the surrouding rocks.

On the top of the CCU described so far, a metasedimentary cover unit occurs. It consists of flysch-like calcschists, devoid of any ophiolite-derived material. They include (although scarce) Qz-rich

micaschists with Grt ± Chl assemblages, Grt-rich calcschists, and meter-sized slivers of Grt-bearing micaceous metaquartzites (see Figure 2). This metasedimentary cover is widespread and occurs in the eastern part of the study area (see Figure 2). In the central portion of the map area the cover unit is nearly absent, but reappears along the western and southern sides of the Lake Miserin. The calcschist ranges in thickness from a few decimeters up to tens of meters. Where the metabreccia unit is thin or absent the calcschist can be directly in contact with serpentinites or the metasomatic horizon, (i.e., to the west), or it can overlie any subunit of the CCU with a total thickness of several meters (i.e., to the east). The compositional layering of calcschists, typically defined by alternating metapelites and marbles (see Figure 3B), is interpreted to correspond to the primary bedding of a post-rift succession (see [19] and Discussion). A dominant feature of these calcschists is the persistent occurrence of millimeter- to centimeter-scale mineral aggregates, pseudomorphs after original Lws, which together with Grt (still preserved) and Cld, indicate a blueschist to eclogite-facies mineral paragenesis.

5. Mesoscale Structural Features

The metaophiolites of the high Champorcher valley have been intensely deformed and metamorphosed under HP then greenschists facies conditions during the Alpine orogeny. Although only one main foliation is recognizable in the field, a polyphase deformation history can be unravelled by integrating structural and microstructural informations from the entire rock sequence. As a general observation, all of the contacts between the different lithologies composing the metaophiolite sequence are near-parallel to each other and to the main foliation due to the transposed nature of earlier-formed deformation features (i.e., D_2; see below).

Within calcschists, the most discernible foliation (here named S_2) retains relict HP-metamorphic mineral phases (mostly concentrated in the micaceous layers) represented by Grt, Cld, and pseudomorphs on Lws, now replaced by Zo/Czo + Wm. The related defomation phase (D_2) is mostly represented by symmetric (Figure 7A) and asymmetric isoclinal folds, from a few centimeters to decimeters in size, which deform an older foliation (S_1) and produce the S_2 axial plane foliation.

In the calcschists, S_1 foliation is interpreted as being due to recrystallization of a sedimentary bedding (S_0), i.e., the primary contact between the carbonate-rich and the micaceous layers (Figure 7A; see also Figure 3B). Due to near complete transposition of earlier fabrics, D_1 structures such as D_1 fold hinges developing S_1 axial plane foliation have never been observed, although we cannot rule out their occurrence (Figure 8).

Within the CCU the most pervasive D_2 structure is represented by the S_2 foliation, that is axial planar to D_2 folds (Figure 7B). S_2 is marked by blueschist to greenschist facies metamorphic minerals such as Srp + Amp + Di + Chl + Cb + Czo + Mag ± Tlc. Within serpentinites and veined serpentinites, the main foliation is marked by the shape preferred orientation (SPO hereafter) of Srp and Chl commonly associated to magnetite.

In the CCU, tight to isoclinal folds, both upright and recumbent, are often associated with strong shearing and boudinaged fold limbs (Figure 7C), where boudinage is developed due to rheological contrasts (e.g., within BrFm2, where ultramafic clasts or layers are embedded in a marble matrix). The contact surface between matrix and boudinaged horizons (likely representing the composite $S_{0/1}$ primary surface) is folded by tight to isoclinal D_1 folds, whose hinges are rarely preserved (Figure 7C; see also Figure 9A for microscopic views). The S_1 foliation is only locally preserved within the ultramafic boudins that are generally highly stretched and elongated in the main foliation S_2 or resemble rootless isoclinal folds. Thus, the S_1 foliation is not pervasively developed within the CCU because it was diffusively overprinted during the D_2 deformation stage. D_2 fold limbs, boudins, and boudin internal foliation are all parallel or sub-parallel to the matrix foliation. Asymmetric or sigmoidal blocks and boudins within the matrix attest for a shear component during D_1/D_2 deformation phases, indicating both top-to NW and top-to NE shear sense, as observed in all the high Champorcher valley. The matrix foliation in all cases cuts the boudinaged layers; due to the shear component during the D_2 phase, the

inside-block foliation is commonly dragged along the block borders, becoming sub-parallel to the matrix foliation (see inset in Figure 7C).

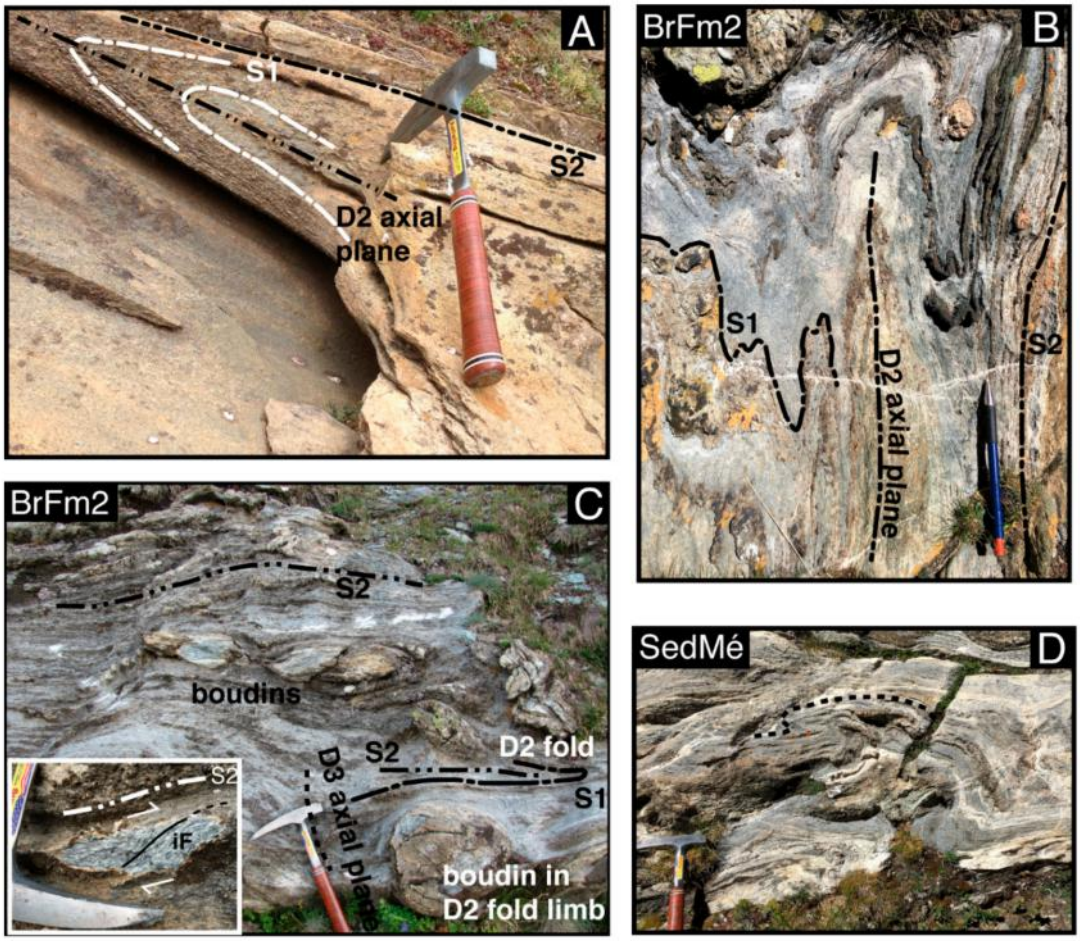

Figure 7. Structural features of the CCU. (**A**) Oldest Alpine foliation S_1 is observed in calcschists which marks the contact between metapelite and marble layers and is interpreted as the original bedding (S_0) of a flyschoid sequence. S_1 foliation has been folded by D_2 isoclinal folds, developing an S_2 axial planar foliation (i.e., the regional-scale main foliation). (**B**) Same S_1-S_2 relations in BrFm2 (northeast of Lake Miserin). (**C**) D_2 phase folding the S_1 foliation in a block-in-matrix fabric (BrFm2). S_1 coincides with the ultramafic boudin/matrix contact and is folded by D_2 folds generating axial planar S_2. D_2 folds have boudinated limbs ("boudins") and are gently re-folded by D_3 phase. Inset: Internal foliation within ultramafic boudin is incorporated into the matrix foliation (S_2). (**D**) Superposed folds generating interference pattern of type 2 of [106] in a SedMé outcrop.

In the study area S_2 schistosity dips moderately towards both the NW and the NE with variable dip angle (ranging between 5° and 75°) (see Figure 2), and exhibits a mineral stretching lineation (L2), defined by lozenge-shaped pseudomorphs on Lws, shallowly plunging (5°–20°) towards the W-NW. The scattering of S_2 attitutes (Figure 2) is due to the asymmetric shape of D_2 structures, and to the superposition of later deformation phases, namely the D_3 phase which produced asymmetric to symmetric, isoclinal to open folds (see Figure 8).

No new axial plane schistosity is developed during the D_3 phase, with the exception of an incipient S_3 in serpentinites and fracture cleavage in calcschists. Within the metasedimentary cover, D_3 folds overprint the pervasive S_2 schistosity, and produce gentle asymmetric open folds, from a few meters to a few decameters in size. D_3 also overprints D_1/D_2 structures in the CCU, producing isoclinal to open folds with subhorizontal axial planes and shallowly plunging fold axes (Figure 2). D_3 fold hinges

trend towards the NW and SW and maintain their shallow plunge (5°–25°) suggesting the effects of late open folding (D_4), characterized by ca N-S-trending fold axes.

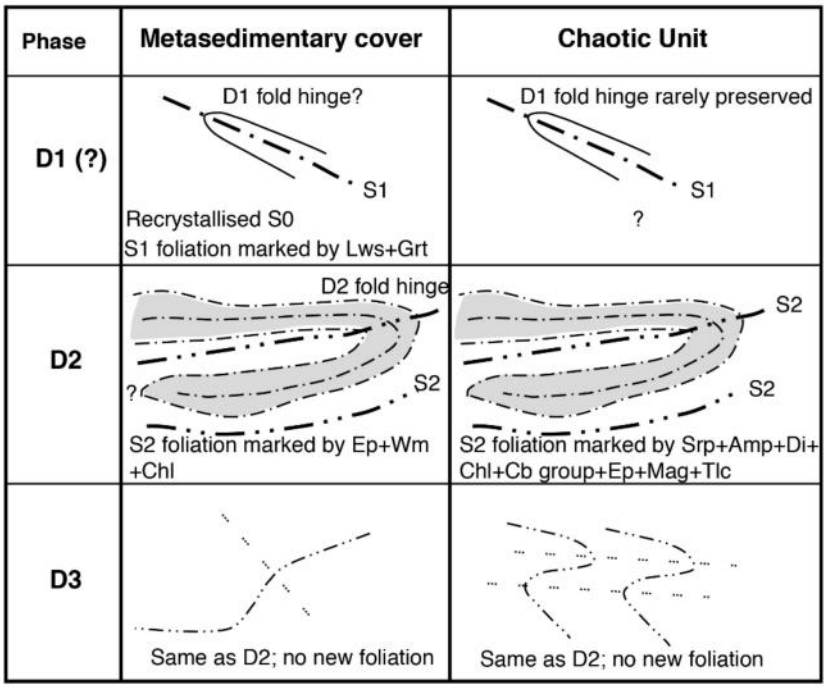

Figure 8. Schematic representation of outcrop scale structures developed in the high Champorcher valley CCU and metasedimentary cover.

Rotation of D_2 fold axes and/or axial planes, as a result of D_3 overprinting, have caused the development of two different types of interference patterns (i.e., "type 1" and "type 2" defined by [106]), according to the structure orientation. One pattern consists of a dome-basin pattern (or type 1) arising from the superposition of two different folding events (i.e., D_2 and D_3 folds), characterized by subparallel axial planes and orthogonal fold axes. A second pattern is a dome-crescent-mushroom pattern (or "type 2") that results from the superposition of D_3 folds on D_2 folds characterized by orthogonal fold axes and orthogonal axial planes (Figure 7D). Such interference patterns enhanced the shape of ultramafic layers and boudins englobed within carbonate-rich matrix in the CCU (see Discussion).

Finally, late-stage brittle deformation produced a variety of structures. Calcschists are diffusively fractured, and fractures isolate rhombohedral rock domain by means of sets of conjugate open fractures, trending NW-NE and SW-W. Within some fractures, an infilling made of Qz ± Chl can be observed. Striated fault planes with fibrous mineralization of Qz or Cal were observed in rare occurrences. Within the CCU, brittle deformation is represented by rare fault planes.

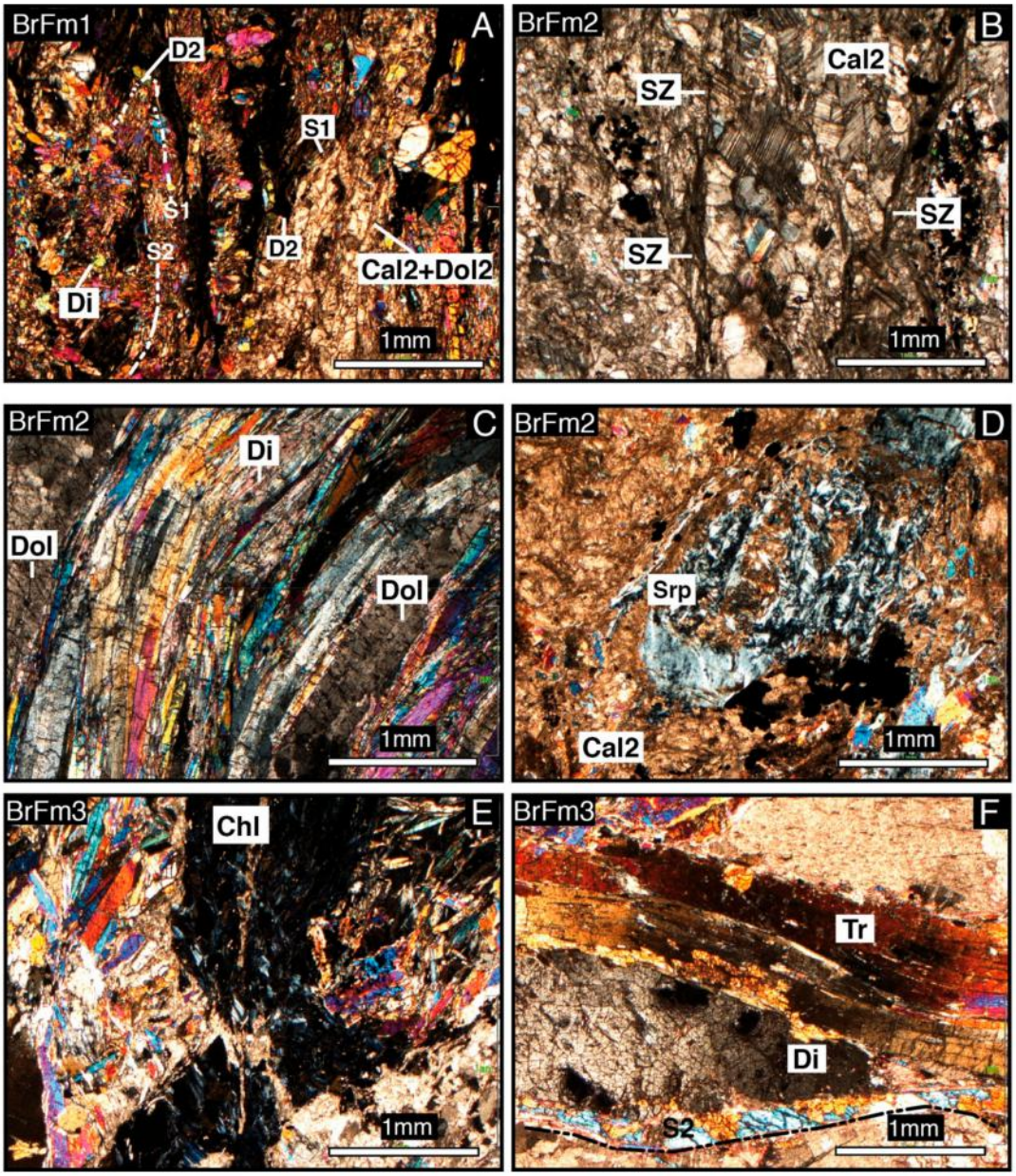

Figure 9. Photomicrographs illustrating the main microstructural features of BrFm1, BrFm2, and BrFm3. All pictures are taken under crossed nicols. Mineral abbreviations after [104]. (**A**) Highly transposed mafic/ultramafic domains and Cb-rich domains in BrFm1 sample. Relict D_2 fold hinges (D_2) are still recognizable. Relict S_1 corresponds to the contact between the two domains. (**B**) Sub-millimeter anastomosing shear zones (SZ) developed in carbonate-rich matrix mainly composed of Cal2 grains. (**C**) lose-up view of minerals filling the boudin neck between ultramafic boudins in BrFm2 (see Figure 7C for outcrop view); Dol and Di crystals are stretched and slightly curved. In the picture the main (S_2) foliation is sub-parallel to crystals. (**D**) Fragment of Srp embedded in Cb-rich matrix in BrFm2 (see text). (**E**) Detail of BrFm3 matrix: elongated or folded layers made of Chl + Opq probably deriving from ultramafic clasts embedded within a carbonate+amphibole-rich matrix. (**F**) Intrafoliar vein in BrFm3. The vein is composed of Amp (Tr), Ep, Cal2/3, and Cpx (Di), this latter forming lenticular aggregates parallel to the S2 foliation planes.

6. Microstructural Features and Petrography

6.1. Serpentinites and Veined Serpentinites

Cb-bearing massive serpentinites (Table S1) are characterized by an incipient S_2 foliation defined by the SPO of fibrous to microcrystalline Srp, lacking any lattice preferred orientation (LPO). Cb includes (i) Dol1 occurring in anhedral sub-cm porphyroclasts, strongly fractured, and dynamically recrystallized into Dol2, and (ii) Dol2 occurring in fine- to medium-grained (sub-mm in size) porphyroblasts, clustered in elongated aggregates. Dol2 occurs locally as pseudomorphs at the expense of earlier pyroxene (probably orthopyroxene), and displays crystalplastic deformation. Opaque minerals (e.g., Mag) occur as crystal trails marking the foliation and as aggregates of crystals with rounded to sub-polygonal shapes.

In foliated serpentinites (Table S2) the S_2 foliated fabric is marked by the SPO of Srp, coincident with its LPO. Several veins, filled with Srp and Opq, occur parallel to the main foliation. Serpentinites in contact with the metasomatic horizon show higher Dol contents (Table S1). The fabric is massive to locally foliated with the S_2 fabric marked by the SPO of Dol aggregates consisting of Dol1 porphyroclasts with intense crystalplastic deformation (undulose extinction), recovery (with subgrains), and dynamical recrystallization with bulging and grain boundary migration. The new grains of Dol2 constitute equigranular aggregates with polygonal contacts, suggesting textural equilibrium [107]. However, Dol2 may display sutured boundaries against Srp fibers which probably grow at the expense of the former, suggesting decarbonation reactions occurring in the carbonated serpentinite [108].

Veined serpentinites (Table S1) consist of serpentinites that are systematically crosscut by various sets of veins that overall overprint the S_2 foliation.

6.2. The Composite Chaotic Unit

6.2.1. BrFm1

In the BrFm1, carbonation of Srp and tectonic transposition frequently mask the internal fabric of the clasts and matrix. Most samples are characterized as having a clast-supported fabric and, due to intense carbonation, it is often difficult to discriminate between the clast and the matrix components. The main (D_2) fabric is a compositional layering defined by the juxtaposition of sub-millimeter-thick layers of Chl ± Ep, Amp2, and of Dol2 + Cal3 (Table S1). Although highly deformed and transposed, D_2 fold hinges are locally preserved (Figure 9A). Relict S_1 foliation is identified as the contact between carbonate-rich and mafic/ultramafic domains.

6.2.2. BrFm2

The BrFm2 is characterized by the occurrence of decimeter-sized boudinaged ultramafic horizons (see Figure 4C for outcrop view) composed of Amp, Chl, Opq, Cpx, and Cb (Table S1). The main foliation is spaced and defined by Opq layers alternating with Chl domains and layers of Cb, Amp, and relict grains of Cpx (probably Di).

The contact between the ultramafic horizons and the marble matrix is often characterized by the development of a shear surface marked by the alignment of Amp + Chl + Opq grains within the ultramafic portion and by Cal3 + Amp + Dol2 fine-grained aggregates within the marble matrix. This points to a strain gradient that was maximized along the contact between the two domains with contrasting rheology.

Within the marble matrix, the S_2 foliation is marked by the SPO of Dol2 + Cal3 and elongated aggregates of Amp ± Chl ± Srp ± Ep. The composition of the matrix may vary from impure to monomineralic. The impure marble matrix has a greyish color and consists of porphyroclastic Cal1, rich in Amp, Chl, and Opq inclusions, dynamically recrystallized into new porphyroblastic Cal2. The monomineralic matrix is white in color and consists of Cal1 occurring in cm-sized porphyroclasts recrystallized into Cal2 porphyroblasts and neoblasts. The Cb-rich matrix is often intersected by sub-millimeter anastomosing shear zones (see Figure 9B).

Isolated ultramafic boudins, likely deriving from stretching of ultramafic horizons, consist of micro-clasts with fibrous aggregates of Srp locally preserving relict a mesh texture, variously associated with fine-grained relics of Cpx and spinel crystals with holly-leaf habit, with the latter being consistent with the mantle origin of their protolith. Srp can be overgrown by micro- to crypto-crystalline Cal3 with dusty brownish aspect suggesting carbonation processes. In spite of carbonation and tectonic transposition, rare relict clastic texture is still recognizable, as evidenced by the occurrence of subrounded serpentinite clasts in sharp contact with a carbonate (Cal2?)-rich domain (Figure 9D). Boudin necks commonly display a foliated texture (S_2) characterized by a continuous coarse-grained foliation, marked by the compositional juxtaposition of mm-thick layers of carbonates and mm-thick layers of pyroxene (Di)-amphibole, stretched in the foliation (Figure 9C).

6.2.3. SedMé

Within foliated rock types of SedMé (see Figure 5A for outcrop view), different fabrics related to different intensities of deformation and/or textural evolution were identified at the micro scale. Representative samples of weakly deformed and tectonitic rocks were selected in order to envisage their composition and fabric evolution (Table S1). Weakly deformed samples consist of ultramafic clasts, cm in size, embedded in a carbonate matrix (Figure 10A). Clasts have tabular to sub-rounded shapes with sharp boundaries, and are locally transposed within the carbonate matrix. Clasts show an internal foliation marked by the SPO of Srp. Foliation inside clasts is often folded or crenulated, with fold hinges developing along the edge of the clast itself. Serpentinitic clasts locally include small Cpx crystals (Di) (Figure 10B) probably derived from recrystallization of original Cpx. The carbonate matrix consists of coarse to medium grained, internally deformed Cal1 porphyrobalsts with interlobate boundaries against the Cal2 neoblasts. Micro- to crypto-crystalline aggregates of Cal2 also fill veins inside the fractured ultramafic clasts.

Tectonites (Table S1) represent the textural evolution of the rock previously described: in fact, the mineralogical composition is similar, except for the presence of Amp, but the fabric is characterized by a continuous foliation (S_2) marked by the SPO of ultramafic clasts or aggregates of clasts (Figure 10C). This evidence points to an incipient development of the S_2 foliation by means of a process of dissolution/precipitation, probably driven by a shear stress which in turn is responsible for the clast fragmentation and the development of flux structures along their boundaries. In spite of this, clasts of serpentinite may preserve relict mesh-like texture, and abrupt truncation of the internal fabric along the clast boundaries, in contact with the matrix (Figure 10D). The Cb-rich matrix in tectonitic samples is characterized by Cal1 relict grains or porphyroclasts (relict with respect to the incipient S_2 foliation, thus related to D_1; Table S1) with diffuse deformation twinning.

The matrix-supported variery of SedMé (see Figure 5B for outcrop view) is characterized by mm to cm ultramafic clasts enveloped in a carbonate matrix. Clasts are commonly transposed within the matrix (Figure 10E), and are extensively carbonated (i.e., Srp is overgrown by Cal3). The carbonate matrix shows either weakly foliated or isotropic granoblastic (almost equibranular) textures. S_2 foliation consists of a compositional layering marked by discontinuous and irregular carbonate layers juxtaposed to Srp + Amp layers. Locally, relics of an earlier foliation (S_1) can be found. These consist of microfolded layers composed of Cal1 and Amp1 (Figure 10F).

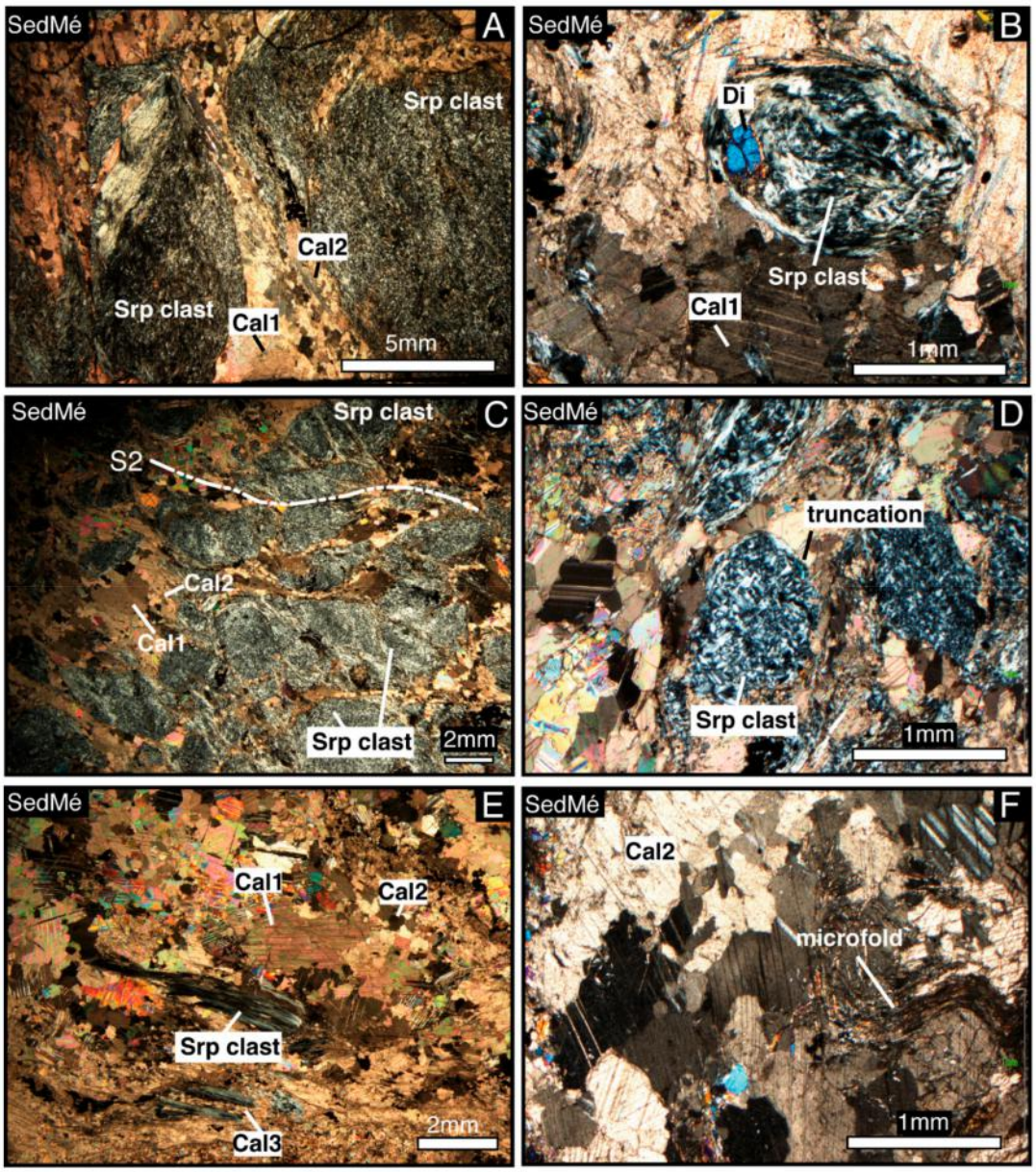

Figure 10. Photomicrographs illustrating the main microstructural features of SedMé. All pictures are taken in crossed-polarized light. Mineral abbreviations after [104]. (**A**) Millimeter- to centimeter-sized ultramafic (serpentinite) clasts embedded in a Cb-rich matrix. Clasts have sub-rounded to elongated shapes. Their boundaries are either truncated or transposed near the contact with the Cb-rich matrix. Clasts on the left show an internal foliation marked by the shape preferred orientation (SPO) of Srp. Foliation is crenulated without the development of a differentiated cleavage. Calcite porphyroblasts (Cal1) and neoblasts (Cal2) are visible in the carbonate-rich matrix. (**B**) Serpentinite clast with Di grain (see text). The clast internal foliation is folded and truncated along the clast margins without drag into the matrix foliation (probably enhanced by dissolution/precipitation). (**C**) Foliated type of SedMé. Foliation (S_2) is defined by SPO of ultramafic clasts or clast aggregates and by carbonate (Cal2) ribbons. Microboudinage of clasts is also recognizable. (**D**) Ultramafic clasts preserving internal relict (or recrystallized) mesh-texture of serpentine. Clasts show either transposed or truncated edges. Truncation is probably enhanced by dissolution/precipitation. (**E**) Matrix-supported type of SedMé characterized by mm- to cm-sized ultramafic clasts diffusively transposed within the matrix consisting of isotropic or weakly foliated fabric. (**F**) Relic of S_1 foliation marked by microfolded layers composed of Cal1 and Amp1 in isotropic types of SedMé.

The SedMé is characterized, differently from the other units, by the (although rare) occurrence of mafic decimeters-sized block (see Figure 5C for outcrop view). These blocks are composed of Amp + Ep + Chl + Ab + Cal. This unit is therefore distinguished by the occurrence of exotic clasts/blocks with different sizes and with ultramafic and mafic composition. Serpentinite clasts are more or less stretched and deformed according to the strain gradient, but always show the abrupt truncation of the internal foliation with resepct to the matrix, this latter being considered diagnostic criteria for recognizing a sedimentary origin of the mélange [15] (see also Discussion).

6.2.4. BrFm3

In the BrFm3, the boudinaged ultramafic horizons (showing various sizes; see Figure 6C for outcrop view) are composed of medium- to fine-grained metasandstone (Table S1). Within the lithics of the metasandstone, the dominant fabric is represented by the SPO of fibrous aggregates of Srp, that define the S_2 foliation, also marked by Opq trails and more rarely by elongated aggregates of fibrous Tlc. The matrix of the metasandstone is characterized by an incipient foliation defined by a compositional layering due to the juxtaposition of sub-mm-thick aggregates of Cal3 and Dol1, two with layers of Cpx, Amp, Ep, Chl, Opq (likely deriving from deformation of ultramafic or mafic clasts; see Figure 9E).

The ultramafic lithics and the matrix are intersected by carbonate/diopside-rich veins which results parallel to the main foliation (i.e., "intrafolial veins"). These veins are composed of Cal, Amp (Tr), Cpx (Di), and Ep (see Figure 9F). The BrFm3, due to its pervasive foliation, tectonic transposition, and mineral recrystallization, is to be considered as the probable product of tectonic reworking of the BrFm2 that is spatially closely associated in the study area (see Figure 2).

6.3. Metasomatic Horizon

The rocks constituting the metasomatic horizon [109] are quite heterogeneous in texture and in modal composition (Table S1). The most diffuse texture is a compositional layering (S_2 foliation) marked by the juxtaposition of Cb-rich and Amp-rich layers. S_2 foliation is axial planar to D_2 folds, whose hinges are locally preserved. C-type shear bands cutting the S_2 foliation are well developed, showing a top-to SW sinistral shear sense.

6.4. Calcschists

Calcschists display a foliated fabric characterized by a continuous to spaced foliation (S_2) marked by the compositional juxtaposition, at varying scales, of Qz + Cal-rich layers (microlithons) alternating with Wm + Chl + Opq-rich layers (cleavage domains; see Table S1). The S_2 foliation displays differing intensities but is never developed into a well-defined spaced foliation with continuous microlithons.

Microlithons are characterized by inequigranular aggregates with polygonal contacts, developed within Cal2 strain-free grains, and interlobate contacts between Cal1 deformed grains and subgrains. Qz (Qz1 porphyrobalsts and Qz2 new grains) is abundant and occurs both as isolated grains within calcite-rich domains, and as fine-grained aggregates. Cleavage domains are dominated by Wm which occurs as Wm1 porphyroclasts (relict with respect to the S_2 foliation) characterized by isolated coarse (millimeters) grain with subhedral shape and rational boundaries, and Wm2 crystals, probably as a result of dissolution/precipitation and dynamic recrystallization mechanisms that contribute to the development of the foliation. Within the microlithons Grt, Ep, and Tur occur in isolated relict grains, wrapped by the S_2 foliation. Evidence of an early foliation (S_1) were observed in one sample where Wm1 + Cal1 + Qz1 mark a foliation (S_1) at a high angle to S_2.

7. Discussion

In exhumed subduction-accretion complexes, the identification of the process (tectonic or sedimentary) of formation of a chaotic rock unit is complicated by the late overprinting of polyphase tectonic deformation and metamorphic recrystallization. Thus, chaotic rock units formed by differing

processes, or by their interlplay and superposition, may be confused and interpreted as the exclusive product of subduction- and/or collisional-related tectonic deformation, underestimating a significant part of their genetic history. This interpretation can prevent a detailed reconstruction of their evolution and an interpretation of their geodynamic setting in which they formed.

Our new detailed structural and petrographic analyses on the HP CCU of the Lake Miserin metaophiolites, allows identification of the role of Alpine tectonic deformation in the formation of such subducted chaotic rock unit. The main purpose is to evaluate the degree of tectonic overprinting and reworking on the CCU primary sedimentary block-in-matrix fabric and the coherent stratigraphic succession formed during the Jurassic rifting stage of the Ligurian-Piedmont oceanic basin [19]. In fact, following [19], the reconstructed primary intra-oceanic depositional setting of the present-day CCU was characterized by alternating carbonate-rich beds and channelized turbidites composed of coarse-grained, clast-to matrix-supported, sandstones/breccias of ultramafic composition (i.e., BrFm2 and BrFm3) formed by gravitational processes triggered by fault scarps dissecting the serpentinized ocean floor. This succession, which is bounded between a metaophiolite sequence made of serpentinite capped by ophicarbonates, and post-rift calcschists, was interbedded by a sedimentary mélange (SedMé), consisting of irregularly shaped serpentinite, ophicalcite, and metamafic blocks randomly distributed within a carbonate-rich matrix.

Our findings demonstrate that the CCU primary stratigraphic succession was overprinted and reworked by a polyphase Alpine tectonic deformation and metamorphic recrystallization. Ductile deformation dominated the prograde subduction-related stage, assisted by fluid circulation in the subduction channel. It is the largely responsible for the reworking and obliteration of the sedimentary fabrics characterizing the CCU. Significantly, the Alpine tectonic deformation was distributed unevenly and with differing intensity within the entire metaophiolite sequence of the high Champorcher valley, and was controlled by the primary or secondary internal texture, organization, and composition. Deformation partitioning may occur on a large variety of scales [110], leaving rock domains characterized by relict and relatively unstrained textures. By applying structural criteria, we compared strained and unstrained domains in the CCU in order to track their fabric evolution.

7.1. Role of Tectonics in the Formation of the CCU

The CCU was affected by at least three main ductile deformation phases, i.e., D_1–D_3 that mostly contributed to the present-day internal fabric.

D_1 structures are not clearly detectable in the field, being recognizable only as relict features. We identified, as the oldest foliation (S_1), the surface marking the lithological contacts in the calcschists and in the CCU: in calcschists, S_1 corresponds to the S_0 sedimentary bedding defined by alternating metapelites and marbles; in the CCU, S_1 corresponds to the lithological contact between ultramafic-rich and carbonate-rich beds, which also could represent an original sedimentary bedding. Finally, internal foliation of clasts and blocks of the CCU are interpreted as S_1, due to its relation to the matrix foliation, always defined as S_2. However, the internal texture of serpentinite clasts (see e.g., Figure 10B,D) may often represent relict oceanic Srp mesh texture.

The subsequent D_2 phase mainly produced isoclinal folding and boudinage that pervasively deformed the S_1 foliation and developed the (axial planar) S_2 foliation recognizable on a regional scale. Since S_1 and S_2 are defined by HP mineral assemblages, then variously re-equilibrated under greenschist-facies conditions, we attributed the D_1–D_2 phases to the subduction stage during which the rocks experienced HP metamorphism.

The D_1–D_2 phases thus played a significant role in reworking the the primary fabrics. These phases are responsible for the stretching, boudinage, and simultaneous folding of the primary stratigraphic succession. Although this deformation affected the entire succession, including the primary sedimentary mélange (i.e., SedMé), it is particularly well-documented and concentrated where differently competent layers are alternate, such as the carbonate-rich and turbiditic ultramafic metasandstone beds in BrFm2 and BrFm3 (see Figures 4–6). Especially within these two latter units,

the D_2 phase has boudinaged this primary stratigraphic layering, aligning the boundary of stretched beds, and/or resulting blocks, parallel or sub-parallel to the S_2 foliation in the carbonate-rich beds. At the higher degree of stratal disruption, the carbonate-rich component represents the matrix of isolated boudinaged to lenticular and/or sigmoidal blocks of ultramafic sandstone (see Figure 4C). The carbonate-rich matrix of both BrFm2 and BrFm3 clearly shows the effect of tectonic reworking and transposition acted upon by the Alpine tectonic phases D_1(?) + D_2, as attested to by the occurrence of stretched mm-thick layers of mafic/ultramafic components clearly transposed from the thicker layers (see Figure 4). Metasomatic minerals (e.g., Di and Tr) are very common along S_2 and in the boudin necks, suggesting that metasomatic reactions between the carbonate and ultramafic components may have occurred during the D_2 phase, assisted by fluids circulating in the subduction zone.

The sigmoidal shape of disrupted ultramafic metasandstone layers in both BrFm2 and BrFm3 attests to a significant shear component during the D_1(?)–D_2 phases. Scaled analogue experiments carried out in a layered medium with rheologically stratified rocks undergoing pure constriction [111], have demonstrated that folds and boudins can interact and grow simultaneously during one single deformation event, at low to moderate finite strain. Moreover, when increasing finite strain, older boudins are affected by later folds and fold limbs are also boudinaged too, giving rise to complex structures resembling those of chaotic rock units (i.e., broken formations). Therefore, the final shape of boudins results from a complex interaction among structures, particularly in a multi-layered system. Due to the shear component during the D_2 phase, the inside block foliation is commonly deformed along the block boundaries, becoming sub-parallel to the matrix foliation (see the inset in Figure 7C).

All of the D_1–D_2 structures have been overprinted by the D_3 deformation phase, which is coeval to the collision and exhumation stages that produced open folds with sub-horizontal fold axes. The superposition of D_3 structures on previously formed structures generated interference patterns (type 1 and type 2 patterns; of [106]), giving rise to resistant spherical to lensoidal blocks as observed mostly in BrFm2 and in some outcrop of SedMé (see Figure 7).

Late stage (post-D_2) shear zones are frequent in the CCU, and are responsible for further dismembering of all previously formed textures (see Figure 9D at the micro scale).

7.2. Origin of the CCU

The BrFm1 of the CCU has a very limited expression in the study area and mainly shows a clast-supported fabric. Commonly, due to the intense tectonic transposition and to carbonation, i.e, carbonate crystallization on serpentine during the subduction-related stage [108], the nature of the primary block-in-matrix fabric of the rocks is difficult to recognize. However, although all the carbonate-rich components in BrFm1 cannot be attributed unambigously to the rock matrix or to late carbonation effect, the occurrence of Cal1, 2, 3 and Dol1, 2, 3 that attesting for a protracted textural evolution, supports the hypothesis that the BrFm1 is derived from a sedimentary (gravitational) process with a limited run-out distance of downslope transport, following in situ stratal disruption related to extensional tectonics and related mechanical fracturing of exhumed mantle rocks on the sea floor (see also [19]).

The block-in-matrix fabric of BrFm2 and BrFm3 can be ascribed to tectonic deformation, at least in part. Similarly, with tectonic serpentinite-matrix mélanges of California (see, e.g., "TSM" defined by [15]), boudinaged horizons of ultramafic metasandstone and isolated lenticular blocks of the same composition show an internal fabric dragged along the block borders towards the matrix foliation. However, the "native" component of boudinaged horizons and lenticular blocks, indicate that BrFm2 and BrFm3 represent broken formations and not mélanges. In fact, their block-in-matrix assemblage formed by the progressive stratal disruption of a primary bedding marked by alternating carbonate-rich and turbidite ultramafic-rich sandstone horizons, acted upon by the various stages of Alpine tectonic deformation (i.e., at least D_1, D_2, and D_3).

In the SedMé, the systematic occurrence of differently evolved fabric in the carbonate-rich matrix, as evidenced by carbonate (Cal1, Dol1) porphyroblasts recrystallized to varying extents into carbonate

neoblasts, and the presence of late Cal3 support the hypothesis of a long-lasting textural evolution of the matrix. Millimeter-sized porphyroblasts observed in some samples might also be reminiscent of an original coarse-grained texture. In addition, serpentinite clasts and blocks, especially those preserving relict mesh texture, show an internal fabric that is truncated along block margins without incorporation into the matrix foliation (see Figure 10D). Truncation along the clast margins probably was enhanced by pressure-solution process during the Alpine tectonic deformation. Similar features have been considered diagnostic of a sedimentary origin of mélanges from the Great Valley Group (California; see [15] and references therein). The random distribution, in the SedMé, of irregularly-shaped clasts and blocks of varying composition (i.e., mafic and ultramafic) within the carbonate-rich matrix, suggest that D_1–D_2 tectonic phases did not completely rework any primary sedimentary (gravitational, see [19]) block-in-matrix fabric. This interpretation is also supported by the evidence that the matrix retains a weakly foliated or isotropic granoblastic fabric (see Figure 4B), with carbonate blasts (commonly Cal2) arranged in a polygonal (almost equiangular) texture. The SedMé shows a scale-invariant random distribution of angular and irregular clasts (see Figure 5C; see also Figure 3D in [19]), a feature diagnostic of a mélange formed through sedimentary (gravitational) processes (i.e., sedimentary mélange) in intra-oceanic settings (see, e.g., referenced [15,22,112]). The irregularly-shaped ultramafic clasts and blocks embedded within the carbonate-rich matrix of SedMé thus represent "exotic" blocks gravitationally collapsed from structural/bathymetric highs (e.g., fault scarp, horst, etc.) exposing both serpentinized peridotite and ophicarbonate. The occurrence of veined serpentinite and ophicarbonate blocks and clasts within SedMé (see also [19]) provides further evidence for exposure of dominant mantle rocks on the seafloor of the Jurassic Tethyan ocean, as observed in modern slow spreading-ridges and in some areas of the Alps and Apennines [17,19,76,80,113]. At slow spreading-ridges the exhumation on the seafloor of mantle rocks leads to their hydration and concurrent involvement in hydrothermal systems: observations of the seafloor have revealed that mafic and ultramafic rocks might be locally associated with carbonate deposits [114,115] thus confirming the genetic hypothesis suggested for the generation of Alpine ophicarbonates.

In all the units in the CCU the most striking feature is the occurrence, inside clasts and blocks, of relict minerals and textures attributable to the original protolith, i.e., mantle peridotite. Opx microstructural sites, holly-leaf spinel and Srp mesh texture are the most prominent (see Figure 10). Spn has a holly-leaf shaped habit typical for spinel crystals of porphyroclastic tectonitic peridotites [116]. Relict mesh texture (or recrystallized mesh texture; see Figure 10D) is ascribable to serpentinization of original Ol crystals in the oceanic environment and/or at the onset of the subduction process of original olivine crystals. Microprobe analyses on these textural and mineralogical relics demonstrated that Spn is zoned with a Cr-rich core and a Fe-rich rim, an observation consistent with the hypothesis of a mantle origin for these serpentinite clasts, and that Srp is mostly Atg (i.e., high temperature/high pressure serpentine phase; see [109,117]). These petrographic observations further support the interpretation presented above regarding the origin of the CCU as the product of superimposed processes gradually disrupting a primary stratigraphic succession deposited on the oceanic seafloor (i.e., OPS) during the Jurassic mantle exhumation.

Further investigations aimed at unravelling the sedimentary vs. tectonic contribution in generating the CCU should be focused on geochemical (mostly isotopic) analyses of the carbonate-rich components. In particular, given the structural investigation reported here, the isotopic signatures should be cross-checked with the structural interpretation.

7.3. Reconstructed Geodynamic Evolution of the CCU

A possible scenario for the genesis and evolution of the CCU is illustrated in the conceptual cartoon illustrated in Figure 11.

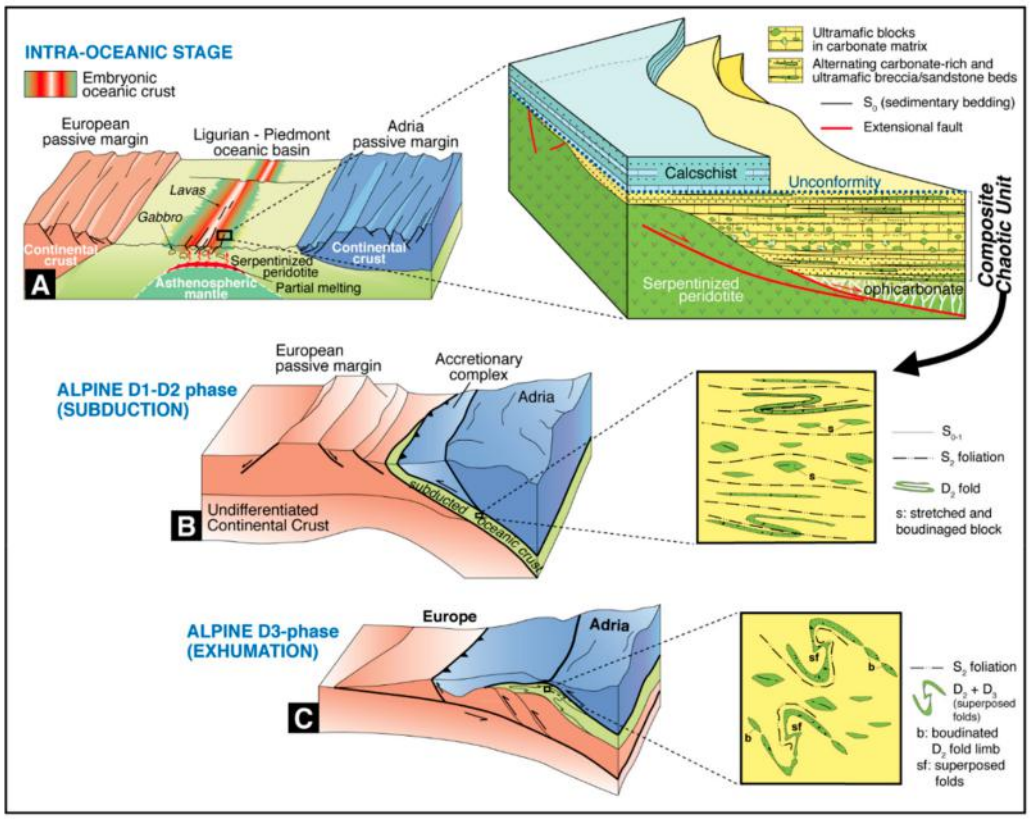

Figure 11. Conceptual cartoon illustrating a possible scenario for the formation and evolution of the CCU. (**A**) Intra-oceanic stage during the syn-extensional tectonics leading to mantle exposure on the seafloor and development of ophicarbonate. The sedimentary succession overlying mantle rocks consists of carbonate-rich sediments alternating with turbidites of ultramafic-rich composition (future BrFm2 and BrFm3), and mass transport deposits (SedMé) with blocks of ultramafic and mafic composition randomly distributed in a carbonate-rich matrix. Calcschists in the block diagram represent a post-rift succession above an unconformity surface. (**B**) Subduction stage dominated by HP D_1–D_2 deformation phases (S_1 and S_2 foliations) that reworked and transposed all previous fabrics by isoclinal folding and boudinage. (**C**) Exhumation stage during which the post-D_2 phases (from D_3 onward) developed are accompanied by greenschist facies mineral recrystallization.

The most likely geodynamic setting for the formation of sedimentary deposits with a block-in-matrix fabric, at Champorcher, begins on the seafloor of the Jurassic Tethyan ocean (or Ligurian-Piedmont ocean) where mantle peridotites + ophicarbonate, intruded by gabbro pockets, were emplaced in an extensional regime (Figure 11A). Extensional tectonics favored the formation of fault scarps and a rough topography, as in modern slow spreading-ridge settings, highly exposed to submarine erosion. Such a setting triggered the inception of mass transport processes and turbiditic sedimentation giving rise to mixed (i.e., ultramafic and carbonatic) deposits with heterogeneous internal fabric. Following the interpretation of [19] we infer that most of the primary internal fabric of the CCU originated during the Jurassic extensional tectonics of the Ligurian-Piedont oceanic basin. Tectono-sedimentary processes related to the exhumation of mantle rocks to the seafloor resulted in the formation of a primary stratigraphic succession (Figure 11A) consisting of turbidite deposits (i.e., future BrFm2 and BrFm3) and mass-transport deposits (SedMé).

The Alpine subduction, dominated by ductile deformation and fluid circulation (Figure 11B), reworked and transposed the internal fabric of the sedimentary deposits. Deformation and mineral recrystallization obliterated textures in the BrFms and SedMé texture. However, by adopting diagnostic criteria for mélange identification [4,15] and classic structural criteria [106], we can identify the contribution of the Alpine tectonics. Indeed, D_1(?) and D_2 phases enhanced the shape of the original

horizons, blocks and clasts by stretching, folding and boudinage (Figure 11B, right side). During exhumation (Figure 11C), late ductile phases (e.g., D_3) were superimposed on D_1 + D_2 structures, giving rise to objects with globular or sub-spherical shapes embedded in a matrix furtherly disrupted by late-stage anastomosing shear zones.

8. Concluding Remarks

Our detailed micro-to meso-structural analysis and petrographic observations idicate that the final block-in-matrix fabric of the CCU occurring in the high Champorcher valley (Lake Miserin sector) represents the contributions of both tectonic and sedimentary (gravitational) processes that accompanied the evolution of a sector of the Jurassic Ligurian-Piedmont ocean basin. This evolution is marked by intra-oceanic deformation (rifting stage), then subduction, collision, and exhumation stages. Polyphase Alpine isoclinal folding, superposition of folds, boudinage and stretching, as well as shearing, created the present features of the CCU through progressive deformation of primary coherent successions (i.e., BrFm2, BrFm3). These subduction- and collision-related processes largely overprinted the primary mass transport deposits (i.e., SedMé), imposing a tectonic foliation on the matrix, deforming and fracturing clasts and blocks. However, although the polyphase Alpine tectonic deformation and metamorphic recrystallization overprinted the primary stratigraphic arrangement of the OPS of this sector of the Ligurian-Piedmont oceanic basin, tectonic reworking mainly acted preferentially (or was recorded) within regular stratigraphic horizons represented by the differing competent layers (i.e., BrFm2 and BrFm3). On the contrary, the isotropic texture of primary sedimentary mélanges (i.e., SedMé) preserved part of its primary diagnostic features from the micro- to the meso-scale.

In conclusion, our findings document that, by the application of specific diagnostic criteria of mélanges geology [4,15], supported by detailed field work, structural and petrographic analyses, it is possible to discriminate the effects of seafloor/protolithic and tectonic processes (subduction, collision, and exhumation) reflected in exhumed orogenic belts and subduction-accretion complexes. These detailed observations, although time-consumming and effort-intensive, can provide significant new constraints toward better understanding of the evolution of the geodynamic setting of mélange formation.

Supplementary Materials: The following are available online at http://www.mdpi.com/2076-3263/9/8/358/s1, Table S1: Schematic relationships between deformation and mineral crystallization in the metaophiolite sequence of the Champorcher valley. Minerals of the CCU include both clasts and the matrix, Text S1: Description of the applied methodologies.

Author Contributions: Conceptualization, P.T., S.G., F.R., A.F., G.B., G.E.B., E.C., G.S.E. and M.S.; methodology, P.T, A.F.; validation, P.T., S.G., F.R., A.F., G.B.; formal analysis, P.T., S.G. and F.R.; investigation, P.T., S.G., F.R.; resources, P.T.; data curation, P.T.; writing—original draft preparation, P.T., S.G., A.F.; writing—review and editing, P.T., A.F. and G.S.E.; visualization, P.T., A.F.; supervision, P.T.; project administration, P.T.; funding acquisition, P.T.

Funding: This research was funded by the Università degli Studi di Milano, grant number PSR2018_DZANONI.

Acknowledgments: I wish to thank the Guest Editor K. Ogata, for inviting me to submit this paper. Two anonymous reviewers are gratefully acknowledged for their constructive revision.

Conflicts of Interest: The authors declare no conflicts of interest.

References

1. Raymond, L.A. Classification of melanges. In *Melanges: Their Nature, Origin and Significance*; Raymond, L.A., Ed.; Geological Society of America: Boulder, CO, USA, 1984; Volume 198, pp. 7–20.
2. Cowan, D.S. Structural styles in Mesozoic and Cenozoic mélanges in the western Cordillera of North America. *Geol. Soc. Am. Bull.* **1985**, *96*, 451–462. [CrossRef]
3. Festa, A.; Pini, G.A.; Dilek, Y.; Codegone, G. Mélanges and mélange-forming processes: A historical overview and new concepts. *Int. Geol. Rev.* **2010**, *52*, 1040–1105. [CrossRef]

4. Festa, A.; Pini, G.A.; Ogata, K.; Dilek, Y. Diagnostic features and field-criteria in recognition of tectonic, sedimentary and diapiric mélanges in orogenic belts and exhumed subduction-accretion complexes. *Gondwana Res.* **2019**. [CrossRef]
5. Berkland, J.O.; Raymond, L.A.; Kramer, J.C.; Moores, E.M.; O'Day, M. What is Franciscan? *Am. Assoc. Petr. Geol. Bull.* **1972**, *56*, 2295–2302.
6. Silver, E.A.; Beutner, E.C. Melanges. *Geology* **1980**, *8*, 32–34. [CrossRef]
7. Raymond, L.A. Perspectives on the roles of melanges in subduction accretionary complexes: A review. *Gondwana Res.* **2019**. [CrossRef]
8. Bettelli, G.; Panini, F. I mélanges dell'Appenino settentrionale dal T. Tresinaro al T. Sillaro. *Mem. Soc. Geol. It.* **1987**, *39*, 187–214.
9. Pini, G.A. *Tectonosomes and olistostromes in the Argille Scagliose of the Northern Apennines, Italy*; Geological Society of America: Boulder, CO, USA, 1999; Volume 335, p. 73.
10. Bettelli, G.; Conti, S.; Panini, F.; Vannucchi, P.; Fioroni, C.; Fregni, P.; Bonacci, M.; Gibellini, R.; Mondani, C. The mapping of chaotic rocks in Abruzzo (Central Italy): Comparison with selected examples from Northern Apennines. In *Mapping Geology in Italy*; Pasquarè, G., Venturini, C., Groppelli, G., Eds.; APAT – SELCA: Firenze, Italy, 2004; pp. 199–206.
11. Alonso, J.L.; Marcos, A.; Suárez, A. Structure and Organization of the Porma Melange: Progressive Denudation of a Submarine Nappe Toe by Gravitational Collapse. *Am. J. Sci.* **2006**, *306*, 32–65. [CrossRef]
12. Festa, A.; Dilek, Y.; Gawlick, H.-J.; Missoni, S. Mass-transport deposits, olistostromes and soft-sediment deformation in modern and ancient continental margins, and associated natural hazards. *Mar. Geol.* **2014**, *356*, 1–4. [CrossRef]
13. Festa, A.; Dilek, Y.; Mittempergher, S.; Ogata, K.; Pini, G.A.; Remitti, F. Does subduction of mass transport deposits (MTDs) control seismic behavior of shallow–level megathrusts at convergent margins? *Gondwana Res.* **2018**, *60*, 186–193. [CrossRef]
14. Wakabayashi, J. Mélanges of the Franciscan Complex, California: Diverse structural settings, evidence for sedimentary mixing, and their connection to subduction processes. In *Melanges: Processes of Formation and Societal Significance*; Wakabayashi, J., Dilek, Y., Eds.; Geological Society of America: Boulder, CO, USA, 2011; Volume 480, pp. 117–141.
15. Wakabayashi, J. Sedimentary compared to tectonically-deformed serpentinites and tectonic serpentinite mélanges at outcrop to petrographic scales: Unambiguous and disputed examples from California. *Gondwana Res.* **2019**. [CrossRef]
16. Dilek, Y.; Festa, A.; Ogawa, Y.; Pini, G.A. Chaos and geodynamics: Mélanges, mélange-forming processes and their significance in the geological record. *Tectonophysics* **2012**, *568*, 1–6. [CrossRef]
17. Balestro, G.; Festa, A.; Dilek, Y.; Tartarotti, P. Pre-alpine extensional tectonics of a peridotite-localized oceanic core complex in the Late Jurassic, High-pressure Monviso ophiolite (Western Alps). *Episodes* **2015**, *38*, 266–282. [CrossRef]
18. Krohe, A. The Franciscan Complex (California, USA) – The model case for return-flow in a subduction channel put to the test. *Gondwana Res.* **2017**, *45*, 282–307. [CrossRef]
19. Tartarotti, P.; Festa, A.; Benciolini, L.; Balestro, G. Record of Jurassic mass transport processes through the orogenic cycle: Understanding chaotic rock units in the high-pressure Zermatt-Saas ophiolite (Western Alps). *Lithosphere* **2017**, *9*, 399–407. [CrossRef]
20. Ogata, K.; Festa, A.; Pini, G.; Pogačnik, Ž.; Lucente, C. Substrate deformation and incorporation in sedimentary mélanges (olistostromes): Examples from the northern Apennines (Italy) and northwestern Dinarides (Slovenia). *Gondwana Res.* **2019**. [CrossRef]
21. Festa, A.; Dilek, Y.; Pini, G.A.; Codegone, G.; Ogata, K. Mechanisms and processes of stratal disruption and mixing in the development of mélanges and broken formations: Redefining and classifying mélanges. *Tectonophysics* **2012**, *568*, 7–24. [CrossRef]
22. Festa, A.; Ogata, K.; Pini, G.A. Mélanges: 100th anniversary of the inception of the term and concept. *Gondwana Res.* **2019**. [CrossRef]
23. Wakita, K. OPS mélange: A new term for mélanges of convergent margins of the world. *Int. Geol. Rev.* **2015**, *57*, 529–539. [CrossRef]
24. Wakabayashi, J. Anatomy of a subduction complex: architecture of the Franciscan Complex, California, at multiple length and time scales. *Int. Geol. Rev.* **2015**, *57*, 669–746. [CrossRef]

25. Wakabayashi, J. Serpentinites and serpentinites: variety of origins and emplacement mechanisms of serpentinite bodies in the California Cordillera. *Island Arc* **2017**, *26*, e12205. [CrossRef]
26. Wakabayashi, J. Structural context and variation of oceanic plate stratigraphy, Franciscan Complex, California: insight into mélange origins and subduction accretion processes. *Progr. Earth Planet. Sci.* **2017**, *4*, 18. [CrossRef]
27. Raymond, L.A. Designating tectonostratigraphic terranes versus mapping rock units in subduction complexes: perspectives from the Franciscan Complex of California, USA. *Int. Geol. Rev.* **2015**, *57*, 801–823. [CrossRef]
28. Cloos, M.; Shreve, R.L. Subduction-channel model of prism accretion melange formation, sediment subduction, and subduction erosion at convergent platemargins: 1. Background and description. *Pure Appl. Geophys.* **1988**, *128*, 455–500. [CrossRef]
29. Guillot, S.; Schwartz, S.; Hattori, K.; Auzende, A.L.; Lardeaux, J.M. The Monviso ophiolitic Massif (Western Alps), a section through a serpentinite subduction channel. *J. Virtual Explor.* **2004**, *16*, 17. [CrossRef]
30. Federico, L.; Crispini, L.; Scambelluri, M.; Capponi, G. Ophiolite mélange zone records exhumation in a fossil subduction channel. *Geology* **2007**, *35*, 499–502. [CrossRef]
31. Roda, M.; De Salvo, F.; Zucali, M.; Spalla, M.I. Structural and metamorphic evolution during tectonic mixing: is the Rocca Canavese Thrust Sheet (Italian Western Alps) a subduction-related mélange? *Ital. J. Geosci.* **2018**, *137*, 311–329. [CrossRef]
32. Balestro, G.; Festa, A.; Borghi, A.; Castelli, D.; Gattiglio, M.; Tartarotti, P. Role of Late Jurassic intra-oceanic structural inheritance in the Alpine tectonic evolution of the Monviso meta-ophiolite Complex (Western Alps). *Geol. Mag.* **2018**, *155*, 233–249. [CrossRef]
33. Dal Piaz, G.V.; Cortiana, G.; Del Moro, A.; Martin, S.; Pennacchioni, G.; Tartarotti, P. Tertiary age and paleostructural inferences of the eclogite-facies imprint in the Austroalpine outliers and Zermatt–Saas ophiolite, western Alps. *Int. J. Earth Sci.* **2001**, *90*, 668–684. [CrossRef]
34. Rebay, G.; Zanoni, D.; Langone, A.; Luoni, P.; Tiepolo, M.; Spalla, M.I. Dating of ultramafic rocks from the Western Alps ophiolites discloses Late Cretaceous subduction ages in the Zermatt-Saas Zone. *Geol. Mag.* **2018**, *155*, 298–315. [CrossRef]
35. Lemoine, M.; Trümpy, R. Pre-oceanic rifting in the Alps. *Tectonophysics* **1987**, *133*, 305–320. [CrossRef]
36. Polino, R.; Dal Piaz, G.V.; Gosso, G. Tectonic erosion at the Adria margin and accretionary processes for the Cretaceous orogeny of the Alps. *Mém. Soc. Géol. Fr.* **1990**, *156*, 345–367.
37. Michard, A.; Goffé, B.; Chopin, C.; Henry, C. Did the Western Alps develop through an Oman-type stage? The geotectonic setting of high-pressure metamorphism in two contrasting Tethyan transects. *EclogaeGeol. Hel.* **1996**, *89*, 43–80.
38. Barnicoat, A. Zoned high-pressure assemblages in pillow lavas of the Zermatt-Saas ophiolite zone, Switzerland. *Lithos* **1988**, *21*, 227–236. [CrossRef]
39. Cartwright, I.; Barnicoat, A.C. Stable isotope geochemistry of Alpine ophiolites: a window to ocean-floor hydrothermal alteration and constraints on fluid-rock interaction during high-pressure metamorphism. *Int. J. Earth Sci.* **1999**, *88*, 219–235. [CrossRef]
40. Fontana, E.; Panseri, M.; Tartarotti, P. Oceanic relict textures in the Mount Avic serpentinites, Western Alps. *Ofioliti* **2008**, *33*, 105–118.
41. Panseri, M.; Fontana, E.; Tartarotti, P. Evolution of rodingitic dykes: Metasomatism amd metamorphism in the Mount Avic serpentinites (Alpine ophiolites, Southern Aosta Valley). *Ofioliti* **2008**, *33*, 165–185.
42. Bearth, P. Die Ophiolithe der Zone von Zermatt-Saas Fee. In *Beitr. Geol. Karte Schweiz (NF)*; Kümmerly & Frey: Lucerna, Switzerland, 1967; p. 130.
43. Dal Piaz, G.V.; Ernst, W.G. Areal geology and petrology of eclogites and associated metabasites of the Piemonte Ophiolite Nappe, Breuil-St. Jacques area, Italian Western Alps. *Tectonophysics* **1978**, *51*, 99–126. [CrossRef]
44. Ernst, W.G.; Dal Piaz, G.V. Mineral parageneses of eclogitic rocks and related mafic schists of Piemonte ophiolite nappe, Breuil-St-Jacques Area, Italian Western Alps. *Am. Mineral.* **1978**, *63*, 621–640.
45. Reynecke, T. Prograde high-to ultrahigh-pressure metamorphism and exhumation of oceanic sediments at Lago di Cignana, Zermatt-Saas zone, western Alps. *Lithos* **1998**, *42*, 147–189. [CrossRef]
46. Groppo, C.; Beltrando, M.; Compagnoni, R. TheP-Tpath of the ultra-high pressure Lago Di Cignana and adjoining high-pressure meta-ophiolitic units: insights into the evolution of the subducting Tethyan slab. *J. Metamorph. Geol.* **2009**, *27*, 207–231. [CrossRef]

47. Rebay, G.; Spalla, M.I.; Zanoni, D. Interaction of deformation and metamorphism during subduction and exhumation of hydrated oceanic mantle: Insights from the Western Alps. *J. Metamorph. Geol.* **2012**, *30*, 687–702. [CrossRef]
48. Luoni, P.; Rebay, G.; Spalla, M.I.; Zanoni, D. UHP Ti-chondrodite in the Zermatt-Saas serpentinite: Constraints on a new tectonic scenario. *Am. Miner.* **2018**, *103*, 1002–1005. [CrossRef]
49. Meyer, J. The development of the high-pressure metamorphism in the Allalin metagabbro (Switzerland). *Terra Cognita* **1983**, *3*, 187.
50. Barnicoat, A.C.; Fry, N. High-pressure metamorphism of the Zermatt-Saas ophiolite zone, Switzerland. *J. Geol. Soc.* **1986**, *143*, 607–618. [CrossRef]
51. Reinecke, T. Very-high-pressure metamorphism and uplift of coesite-bearing metasediments from the Zermatt-Saas zone, Western Alps. *Eur. J. Miner.* **1991**, *3*, 7–18. [CrossRef]
52. Bucher, K.; Fazis, Y.; De Capitani, C.; Grapes, R. Blueschists, eclogites, and decompression assemblages of the Zermatt-Saas ophiolite: High-pressure metamorphism of subducted Tethys lithosphere. *Am. Miner.* **2005**, *90*, 821–835. [CrossRef]
53. Angiboust, S.; Agard, P.; Jolivet, L.; Beyssac, O. The Zermatt-Saas ophiolite: the largest (60-km wide) and deepest (c.70–80 km) continuous slice of oceanic lithosphere detached from a subduction zone? *Terra Nova* **2009**, *21*, 171–180. [CrossRef]
54. Dale, C.W.; Burton, K.W.; Pearson, D.G.; Gannoun, A.; Alard, O.; Argles, T.W.; Parkinson, I.J. Whole rock and mineral-scale insights from a high-pressure terrain. *Geochim. Cosmochim. Ac.* **2009**, *73*, 1394–1416. [CrossRef]
55. Vannay, J.-C.; Allemann, R. La zone piémontaise dans le Haut-Valtournanche Val d'Aoste, Italie. *Eclogae Geol. Hel.* **1990**, *83*, 21–39.
56. Caby, R.; Kienast, J.R.; Saliot, P. Structure, métamorphisme et modèle d'évolution tectonique des Alpes occidentale. *Rev. Géogr. Phys. Géol. Dyn.* **1978**, *20*, 307–322.
57. Ayrton, S.; Bugnon, C.; Haarpainter, T.; Weidmann, M.; Frank, E. Geologie du fron de la nappe de la Dent Blanche dans la region des Monts-Dolins, Valais. *Eclogae Geol. Helv.* **1982**, *75*, 269–286.
58. Desmons, J. Different metamorphic evolutions in the Alpine-Apenninic ophiolites (France-Italy-Switzerland-Austria). *Chem. Geol.* **1989**, *77*, 229–250. [CrossRef]
59. Festa, A.; Balestro, G.; Dilek, Y.; Tartarotti, P. A Jurassic oceanic core complex in the high-pressure Monviso ophiolite (western Alps, NW Italy). *Lithosphere* **2015**, *7*, 646–652. [CrossRef]
60. Dewey, J.F.; Helman, M.L.; Knott, S.D.; Turco, E.; Hutton, D.H.W. Kinematics of the western Mediterranean. *Geol. Soc. Lond. Spec. Publ.* **1989**, *45*, 265–283. [CrossRef]
61. Rubatto, D.; Gebauer, D.; Fanning, M. Jurassic formation and Eocene subduction of the Zermatt-Saas-Fee ophiolites: implications for the geodynamic evolution of the Central and Western Alps. *Contrib. Miner. Pet.* **1998**, *132*, 269–287. [CrossRef]
62. Stampfli, G.; Borel, G.; Marchant, R.; Mosar, J. Western Alps geological constraints on western Tethyan reconstructions. *J. Virtual Explor.* **2002**, *8*, 75–104. [CrossRef]
63. Spalla, M.I.; Lardeaux, J.M.; Piaz, G.V.D.; Gosso, G.; Messiga, B. Tectonic significance of Alpine eclogites. *J. Geodyn.* **1996**, *21*, 257–285. [CrossRef]
64. Dal Piaz, G.V.; Bistacchi, A.; Massironi, M. Geological outline of the Alps. *Episodes* **2003**, *26*, 175–180.
65. Beltrando, M.; Rubatto, D.; Manatschal, G. From passive margins to orogens: The link between ocean-continent transition zones and (ultra)high-pressure metamorphism. *Geology* **2010**, *38*, 559–562. [CrossRef]
66. Lardeaux, J.-M. Deciphering orogeny: a metamorphic perspective. Examples from European Alpine and Variscan belts: Part I: Alpine metamorphism in the western Alps. A review. *Bull. Soc. Géol. Fr.* **2014**, *185*, 93–114. [CrossRef]
67. Rubatto, D.; Regis, D.; Hermann, J.; Boston, K.; Engi, M.; Beltrando, M.; McAlpine, S.R.B.; Hermann, J. Yo-yo subduction recorded by accessory minerals in the Italian Western Alps. *Nat. Geosci.* **2011**, *4*, 338–342. [CrossRef]
68. Manzotti, P.; Ballèvre, M.; Zucali, M.; Robyr, M.; Engi, M. The tectonometamorphic evolution of the Sesia–Dent Blanche nappes (internal Western Alps): Review and synthesis. *Swiss J. Geosci.* **2014**, *107*, 309–336. [CrossRef]
69. Hunziker, J.C. Rb-Sr and K-Ar age determination and the Alpine tectonic history of the western Alps. *Mem. Ist. Geol. Mineral. Univ. Padova* **1974**, *31*, 54.
70. Rubatto, D.; Gebauer, D.; Compagnoni, R. Dating of eclogite-facies zircons: The age of Alpine metamorphism in the Sesia–Lanzo Zone (Western Alps). *Earth Planet. Sci. Lett.* **1999**, *167*, 141–158. [CrossRef]

71. Roda, M.; Spalla, M.I.; Marotta, A.M. Integration of natural data within a numerical model of ablative subduction: a possible interpretation for the Alpine dynamics of the Austroalpine crust. *J. Metamorph. Geol.* **2012**, *30*, 973–996. [CrossRef]
72. Stöckhert, B.; Gerya, T.V. Pre-collisional high pressure metamorphism and nappe tectonics at active continental margins: a numerical simulation. *Terra Nova* **2005**, *17*, 102–110. [CrossRef]
73. Dal Piaz, G.V. La formazione mesozoica dei calcescisti con pietre verdi fra la Valsesia e la Valtournanche ed i suoi rapporti con il ricoprimento Monte Rosa e con la Zona Sesia-Lanzo. *Boll. Soc. Geol. It.* **1965**, *84*, 67–104.
74. Bocchio, R.; Benciolini, L.; Martin, S.; Tartarotti, P. Geochemistry of eclogitised Fe-Ti gabbros from various lithological settings (Aosta Valley ophiolites, Italian western Alps). Protolith composition and eclogite-facies paragenesis. *Period. Mineral.* **2000**, *69*, 217–237.
75. Dal Piaz, G.V.; Pennacchioni, G.; Tartarotti, P.; Carraro, F.; Gianotti, F.; Monopoli, B.; Schiavo, A. Carta Geologica d'Italia, Foglio 091 Chatillon Servizio. *Geologico d'Italia, Foglio* **2010**, *91*, 5–152.
76. Lombardo, B.; Nervo, R.; Compagnoni, R.; Messiga, B.; Kienast, J.; Mével, C.; Fiora, L.; Piccardo, G.; Lanza, R. Osservazioni preliminari sulle ofioliti metamorfiche del Monviso (Alpi Occidentali). *Rend. Soc. Ital. Mineral. Petrol.* **1978**, *34*, 253–305.
77. Balestro, G.; Fioraso, G.; Lombardo, B. Geological map of the Monviso massif (Western Alps). *J. Maps* **2013**, *9*, 623–634. [CrossRef]
78. Brovarone, A.V.; Herwartz, D. Timing of HP metamorphism in the Schistes Lustrés of Alpine Corsica: New Lu–Hf garnet and lawsonite ages. *Lithos* **2013**, *172*, 175–191. [CrossRef]
79. Lagabrielle, Y.; Brovarone, A.V.; Ildefonse, B. Fossil oceanic core complexes recognized in the blueschist metaophiolites of Western Alps and Corsica. *Earth Sci. Rev.* **2015**, *141*, 1–26. [CrossRef]
80. Balestro, G.; Festa, A.; Dilek, Y. Structural architecture of the Western Alpine Ophiolites, and the Jurassic seafloor spreading tectonics of the Alpine Tethys. *J. Geol. Soc.* **2019**. [CrossRef]
81. Frisch, W. Tectonic progradation and plate tectonic evolution of the Alps. *Tectonophysics* **1979**, *60*, 121–139. [CrossRef]
82. Trümpy, R. *An outline of the geology of Switzerland*; Guide Book G10, Part A; Int. Géol. Congr. Wepf & Co.: Basel, Switzerland, 1980; Volume 26, p. 104.
83. Lemoine, M. Structuration jurassique des Alpes occidentales et palinspastique de la Téthys ligure. *Bull. Soc. Géol. Fr.* **1985**, *1*, 126–137.
84. Ballevre, M.; Manzotti, P.; Piaz, G.V.D. Pre-Alpine (Variscan) Inheritance: A Key for the Location of the Future Valaisan Basin (Western Alps). *Tectonics* **2018**, *37*, 786–817. [CrossRef]
85. Colombi, A.; Pfeifer, H.-R. Ferrogabbroic and basaltic meta-eclogites from the Antrona mafic-ultramafic complex and the Centovalli-Locarno region (Italy and Southern Switzerland) - first results. *Schweiz. Mineral. Petrogr. Mitt.* **1986**, *66*, 99–110.
86. Keller, L.M.; Schmid, S.M. On the kinematics of shearing near the top of the Monte Rosa nappe and the nature of the Furgg zone in Val Loranco (Antrona valley, N. Italy): tectonometamorphic and paleogeographical consequences. *Schweiz. Mineral. Petrogr. Mitt.* **2001**, *81*, 347–367.
87. Turco, F.; Tartarotti, P. The Antrona nappe: lithostratigraphy and metamorphic evolution of ophiolites in the Antrona valley (Pennine Alps). *Ofioliti* **2006**, *31*, 207–221.
88. Elter, G. Contribution a la connaissance du Briançonnais interne et de la bordure piémontaise dans les Alpes Graies nord-orientales et considérations sur les rapports entre les zones du Briançonnais et des Schistes Lustrés. *Mem. Ist. Geol. Min. Univ. Padova* **1972**, *28*, 19.
89. Lemoine, M.; Boillot, G.; Tricart, P. Ultramafic and gabbroic ocean floor of the Ligurian Tethys (Alps, Corsica, Apennines): in search of a genetic model. *Geology* **1987**, *15*, 622–625. [CrossRef]
90. Liati, A.; Froitzheim, N.; Fanning, C.M. Jurassic ophiolites within the Valais domain of the Western and Central Alps: geochronological evidence for re-rifting of oceanic crust. *Contrib. Miner. Pet.* **2005**, *149*, 446–461. [CrossRef]
91. Martin, S.; Tartarotti, P.; Dal Piaz, G.V. The Mesozoic ophiolites of the Alps: A review. *Boll. Geofis. Teor. Appl.* **1994**, *36*, 141–144.
92. Weissert, H.J.; Bernoulli, D. A transform margin in the Mesozoic Tethys: Evidence from the Swiss Alps. *Acta Diabetol.* **1985**, *74*, 665–679. [CrossRef]
93. Bearth, P.; Schwander, H. The post-triassic sediments of the ophiolite zone Zermatt-Saas Fee and the associated manganese mineralization. *Ecl. Geol. Helv.* **1981**, *74*, 189–205.

94. Frezzotti, M.L.; Selverstone, J.; Sharp, Z.D.; Compagnoni, R. Carbonate dissolution during subduction revealed by diamond-bearing rocks from the Alps. *Nat. Geosci.* **2011**, *4*, 703–706. [CrossRef]
95. Beltrando, M.; Hermann, J.; Lister, G.; Compagnoni, R.; Hermann, J. On the evolution of orogens: Pressure cycles and deformation mode switches. *Earth Planet. Sci. Lett.* **2007**, *256*, 372–388. [CrossRef]
96. Beltrando, M.; Lister, G.; Hermann, J.; Forster, M.; Compagnoni, R.; Hermann, J. Deformation mode switches in the Penninic units of the Urtier Valley (Western Alps): Evidence for a dynamic orogen. *J. Struct. Geol.* **2008**, *30*, 194–219. [CrossRef]
97. Beltrando, M.; Lister, G.S.; Forster, M.; Dunlap, W.J.; Fraser, G.; Hermann, J.; Hermann, J. Dating microstructures by the 40Ar/39Ar step-heating technique: Deformation–pressure–temperature–time history of the Penninic Units of the Western Alps. *Lithos* **2009**, *113*, 801–819. [CrossRef]
98. Gosso, G.; Benciolini, L.; Dilek, Y.; Festa, A.; Spalla, M.I.; Tartarotti, P. Structural and metamorphic evolution of an ocean-continent transition (OCT) zone mélange deformed under HP conditions during Alpine subduction (Western Italian Alps). In Proceedings of the AGU Fall Meeting Abstract, San Francisco, CA, USA, 5–9 December 2011.
99. Ellero, A.; Loprieno, A. Nappe stack of Piemonte-Ligurian units south of Aosta Valley: New evidence from Urtier Valley (Western Alps). *Geol. J.* **2017**, *53*, 1665–1684. [CrossRef]
100. Fontana, E.; Tartarotti, P.; Panseri, M.; Buscemi, S. Geological map of the Mount Avic massif (Western Alps Ophiolites). *J. Maps* **2015**, *11*, 126–135. [CrossRef]
101. Driesner, T. Aspects of petrographical, structural and stable isotope geochemical evolution of ophicarbonate breccias from ocean floor to subduction and uplift; an example from Chatillon, Middle Aosta Valley, Italian Alps. *Schweiz. Mineral. Petrogr. Mitt.* **1993**, *73*, 69–84.
102. Tartarotti, P.; Benciolini, L.; Monopoli, B. Brecce serpentinitiche nel massiccio ultrabasico del Monte Avic (Falda Ofiolitica Piemontese): possibili evidenze di erosione sottomarina. *Atti Tic. Sc. Terra* **1998**, *7*, 73–86.
103. Dal Piaz, G.V. The Austroalpine-Piedmont nappe stack and the puzzle of Alpine Tethys. In *Third workshop on alpine geology, Biella-Oropa 1997*; Gosso, G., Jadoul, F., Sella, M., Spalla, M.I., Eds.; Memorie di Scienze Geologiche: Roma, Italy, 1999; Volume 51, pp. 155–176.
104. Whitney, D.L.; Evans, B.W. Abbreviations of names of rock-forming minerals. *Am. Mineral.* **2010**, *95*, 185–187. [CrossRef]
105. Bogoch, R. Classification and genetic models of ophicarbonate rocks. *Ofioliti* **1987**, *12*, 23–36.
106. Ramsay, J.G.; Huber, M.I. *The techniques of modern structural geology: Folds and Fractures*; Elsevier Science: London, UK, 1997.
107. Passchier, C.W.; Trouw, R.A.J. *Microtectonics*, 2nd ed.; Springer-Verlag: Berlin, Germany, 2005; p. 366.
108. Scambelluri, M.; Bebout, G.E.; Belmonte, D.; Gilio, M.; Campomenosi, N.; Collins, N.; Crispini, L. Carbonation of subduction-zone serpentinite (high-pressure ophicarbonate; Ligurian Western Alps) and implications for the deep carbon cyclcing. *Earth Planet. Sci. Lett.* **2016**, *441*, 155–166. [CrossRef]
109. Rotondo, F. The Metasomatic Reaction Rim between Serpentinites and Metasediments in the High Champorcher Valley Metaophiolite (Aosta Valley, Western Alps): Structural and Petrographic Features and Inference for the Oceanic and Subduction Evolution. Master's Thesis, Università degli Studi di Milano, Milano, Italy, December 2018.
110. Bell, T.H. Deformation partitioning and porphyroblast rotation in metamorphic rocks: A radical reinterpretation. *J. metamorphic Geol.* **1985**, *3*, 109–118. [CrossRef]
111. Zulauf, J.; Zulauf, G. Coeval folding and boudinage in four dimensions. *J. Struct. Geol.* **2005**, *27*, 1061–1068. [CrossRef]
112. Festa, A.; Ogata, K.; Pini, G.A.; Dilek, Y.; Alonso, J.L. Origin and significance of olistotromes in the evolution of orogenic belts: a global synthesis. *Gondwana Res.* **2016**, *39*, 180–203. [CrossRef]
113. Frassi, C.; Musumeci, G.; Zucali, M.; Mazzarini, F.; Rebay, G.; Langone, A. The Cotoncello Shear Zone (Elba Island, Italy): The deep root of a fossil oceanic detachment fault in the Ligurian ophiolites. *Lithos* **2017**, *278–281*, 445–463. [CrossRef]
114. Früh-Green, G.L.; Kelley, D.S.; Bernasconi, S.M.; Karson, J.A.; Ludwig, K.A.; Butterfield, D.A.; Boschi, C.; Proskurowski, G. 30,000 Years of Hydrothermal Activity at the Lost City Vent Field. *Science* **2003**, *301*, 495–498. [CrossRef] [PubMed]
115. Denny, A.R.; Kelley, D.S.; Früh-Green, G.L. Geological evolution of the Lost City Hydrothermal Field. *Geochem. Geophy. Geosy.* **2015**, *17*, 375–394. [CrossRef]

116. Mercier, J.-C.C.; Nicolas, A. Textures and fabrics of upper-mantle peridotites as illustrated by xenoliths from basalts. *J. Petrol.* **1975**, *16*, 454–487. [CrossRef]
117. Guerini, S.S.G. Multi-Scale Structural Analysis of a Chaotic Rock Unit in the High-Pressure Zermatt-Saas Ophiolite (Western Alps). Master's Thesis, Università degli Studi di Milano, Milano, Italy, July 2018.